Experimental Study of Gas-Induced Liquid-Flow Structures in Bubble Columns

S. Degaleesan, M. Dudukovic, and Y. Pan
Chemical Reaction Engineering Laboratory, Dept. of Chemical Engineering, Washington University, St. Louis, MO 63130

The computer-automated radioactive-particle tracking (CARPT) technique is used to investigate liquid recirculation and turbulence in bubble columns. Experiments are conducted in air–water bubble columns of different sizes, with various gas distributors, and operated over a range of superficial gas velocities. This study covers gas–liquid flows from the bubbly regime to the churn turbulent regime. The time-averaged spatial flow structure, axial liquid velocity profiles, Reynolds shear stress, and turbulence intensities profiles are analyzed for different columns and flow conditions. Supplementary experiments, using the hot-probe anemometry technique, are performed at selected flow conditions, and the results are compared with the corresponding ones from CARPT measurements. The Reynolds stress determined by CARPT was compared with that obtained by hot-film anemometry in an independent investigation by Menzel et al. (1990).

Introduction

Bubble columns are cylindrical vessels wherein gas is sparged, via a distributor, in the form of bubbles, into liquid or liquid–solid suspension. Bubble columns serve as multiphase contactors and reactors in the chemical, petrochemical, biochemical, and metallurgical industries. As reactors, bubble columns are used for chemical processes involving oxidation, chlorination, alkylation, polymerization, and hydrogenation reactions (Shah et al., 1982; Fan, 1989). Other processes that employ bubble columns include hydrotreating and conversion of petroleum residues and direct and indirect liquefaction in the production of liquid fuels from coal. Bubble columns have been identified as a suitable type of reactor for a variety of gas conversion processes involving the production of liquid fuels from synthesis gas. Typical examples are the Fischer-Tropsch process, synthesis of methanol, and manufacture of other synthetic fuels that offer environmental advantages over petroleum-derived fuels. Technology for the liquid-phase methanol synthesis in slurry bubble columns has been recently developed. Bubble columns also have found wide application as fermentors, in wastewater treatment, and in a variety of metallurgical operations such as leaching of metal ores. Excellent heat- and mass-transfer characteristics, lack of moving parts, and therefore reduced wear and tear, higher durability of catalyst, ease of operation, compactness, and low operating and maintenance costs are the advantages that render bubble columns as an attractive reactor choice for various multiphase processes, especially for processes involving highly exothermic reactions.

Bubble columns usually operate with a length-to-diameter ratio, or aspect ratio, of at least five. They are operated in either semibatch (zero liquid throughput) or continuous mode (cocurrent or countercurrent flow of gas and liquid), with liquid superficial velocities lower than the gas superficial velocity by at least an order of magnitude. As a result, it is the flow of gas that controls the hydrodynamics of the individual phases in these systems. In the presence of a solid (catalyst) phase, these reactors are commonly referred to as slurry bubble columns. The size of particles used in slurry bubble columns are typically in the range of 5 to 100 μm, with a solids loading of up to 50% by weight (Krishna et al., 1997). Heat-exchanger tubes can be inserted into the reactor for cooling the system and maintaining isothermal conditions, especially for highly exothermic reactions. In addition, in some cases the column may be sectionalized using baffles to inhibit liquid back mixing (Shah et al., 1982; Deckwer and Schumpe, 1993).

Correspondence concerning this article should be addressed to M. Dudukovic.
Present address of S. Degaleesan, Shell Oil Company, Houston, TX.
Current address of Y. Pan: Toyota Central R&D Labs, Inc., Nagoya, Japan.

In general, the design and scale-up of bubble-column reactors depends on the quantification of three main phenomena: (1) heat and mass transfer, (2) mixing characteristics; and (3) chemical kinetics of the reacting system. The first two are system dependent and intimately linked with the fluid dynamics of bubble columns. Although simple in construction, due to the complex hydrodynamics and its influence on transport characteristics, the design and scale-up of bubble columns has involved considerable empiricism, and has been the subject of extensive ongoing research (Shah et al., 1982; Deckwer and Schumpe, 1993; Saxena, 1995; Dudukovic et al., 1991, 1999; Fan, 1989). Reported studies indicate that the accurate and successful design and scale-up of bubble-column reactors requires an improved understanding of the multiphase fluid dynamics and its influence on phase holdup distribution, mixing, and transport characteristics.

In recent years considerable effort has been directed toward fundamental fluid-dynamic modeling of two-phase flows in bubble-columns with the aim of using these models as tools in the design of bubble-column reactors. This has resulted in a number of computational fluid dynamics (CFD) studies (Svendsen et al., 1992; Ranade, 1992; Grienberger and Hofmann, 1992; Sokolichin and Eigenberger, 1994; Lapin and Lubbert, 1994; Delnoij et al., 1997; Pan et al., 1999, 2000; Sanyal et al., 1999). However, the uncertainty regarding the various phase interaction terms and turbulence closure schemes, in addition to the computational difficulties associated with computation of large flow fields, have in practice delayed the full implementation of CFD codes. Simulation of the churn-turbulent flow regime, which is preferred for industrial bubble columns, poses further difficulties due to the complications arising from the multiple bubble sizes and bubble interactions.

It is widely recognized that the present fluid-dynamic models used in the numerical simulation of bubble columns require experimental data as input and for model verification. In general, the flow in a bubble column is highly turbulent, and the instantaneous flow patterns tend to lack symmetry about the central axis. Therefore, one would expect the need for a 3-D simulation to capture the dynamic features of the flow field. These computations are, however, costly and time-consuming to run. Hence, until recently, most reported CFD studies of bubble columns were based on the 2-D axisymmetric assumption, which results in the computed liquid–phase flow field that exhibits a single-cell recirculation pattern with upflow in the center and downflow at the walls (Grienberger and Hofmann, 1992; Lapin and Luebbert, 1994; Kumar et al., 1995a; Sokolichin et al., 1997; Pan and Dudukovic, 1999, 2000). Serving as a simplified means of simulating the full 3-D flow, the 2-D axisymmetric simulations can be, if properly validated, useful for engineering calculations of the overall velocity and gas holdup distribution (Krishna et al., 2000). Moreover, the results also provide the basis for the development and improvement of 1-D models, as widely used in the design of bubble columns employed in F-T synthesis and other gas conversion processes. However, a 2-D simulation cannot capture the dynamic features of the flow, such as the spiral motions (Krishna et al., 2000; Sanyal et al., 1999). It is important to examine the effect of neglecting these features on the prediction of the overall reactor flow field and performance. A satisfactory answer to these issues only can be obtained through a detailed comparison between the experimental data and simulations. Hence, the efforts in modeling and simulation have to be supplemented with reliable experimental data for the fluid-dynamic parameters describing phase velocities, phase interaction, and turbulence.

Numerous experimental studies have been conducted to provide insight into gas holdup and liquid-velocity distribution in bubble columns. Notable among these is the early study by Hills (1974), who, using pilot tubes, provided the radial profiles of liquid velocity at different gas superficial velocity. His measurements were among the first for local averaged liquid velocities and holdup in bubble columns. Other investigations used invasive and/or local probes such as flywheel anemometer (Nottenkamper et al., 1983), heat-pulse anemometry (Lubbert and Larson, 1990), hot-film anemometry (Delhaye, 1969; Serizawa et al., 1975; Herringe and Davis, 1974; Franz et al., 1984; Menzel et al., 1990; Yao et al., 1991). The laser doppler anemometry, which is a noninvasive technique, had been used by Groen et al. (1995, 1996) and Mudde et al. (1997a,b) to obtain liquid velocities at designated locations of the columns. Fan and coworkers (Tzeng et al., 1993; Chen et al., 1994; Lin et al., 1996; Mudde et al., 1997a) introduced particle image velocimetry (PIV), which is also a noninvasive technique, to measure the liquid velocity field and flow structure in, mainly 2-D, bubble columns. While all of these investigations provided valuable insight into the flow structure in bubble columns, the techniques employed have several shortcomings. They are cumbersome to use in large-diameter columns; it is very difficult and extremely time-consuming to map the flow field in the entire column; they fail at large-volume fractions of the dispersed phase, and yet it is the operation in churn turbulent flow at high gas holdup that is of current industrial interest. In contrast, Devanathan et al. (1990) and Devanathan (1991) introduced radioactive particle tracking for studies of liquid motion in bubble columns. This technique is capable of providing the flow field in the whole column in a reasonable period of time, can handle large-diameter columns, and most importantly is not hindered by and is fully operational in systems with high-volume fraction of the gas. Moreover the radioactive-particle tracking technique produces Lagrangian data for the whole column.

Providing a reliable experimental database for the liquid-phase fluid-dynamic parameters under various conditions by using the computer-automated radioactive-particle tracking (CARPT) technique is the main objective of the present investigation. Such a goal is achieved by conducting CARPT experiments in bubble columns of three sizes—14 cm, 19 cm, and 44 cm in diameter—to study the effects of scale, operating conditions, and gas distributor (sparger) on the fluid dynamic parameters in the air–water system. The parameters measured using CARPT (in the entire flow field) include the ensemble averaged liquid velocities, turbulence properties such as Reynolds stresses and turbulence intensities, and the turbulent eddy diffusivities.

Liquid-phase mixing is one of the important factors in the design of bubble-columns reactors, which not only governs the residence-time distribution of the liquid, but also affects that of the gas phase, and in addition, determines the mean driving force for mass transfer. One of the advantages of the

CARPT technique, in comparison with other velocity measurement techniques, such as particle image velocimetry (PIV) and laser doppler anemometry (LDA), lies in its Lagrangian nature, which results in the ability to directly measure the turbulent eddy diffusivities. Such experimental information can be utilized to study and model the effect of fluid dynamics on liquid-phase mixing in bubble columns. In the present article, however, we focus on the fluid-dynamics aspects of the liquid-phase flow field and leave the topic of liquid-phase mixing to a subsequent article.

Computer-Automated Radioactive-Particle Tracking Technique

The (CARPT) technique is a noninvasive technique for tracking the trajectory of a radioactive particle moving along with a continuous media flow. Originally, the technique was developed by Lin et al. (1985) for the study of solids motion in gas–fluidized beds. Undergoing a number of refinements, this technique has been adapted by Devanathan (1990), Dudukovic et al. (1991), and Yang et al. (1992) for the study of liquid motion and mixing in bubble columns. In the CARPT technique the position of a neutrally buoyant radioactive particle, which follows the liquid phase, is located, by means of measuring the radioactive intensity received from the particle, at a certain frequency over a certain period of time. To illustrate the tracer particle motion in a bubble column, we reconstructed, directly from an actual CARPT experiment, a small segment of particle position data as a function of time. Such a segment of the particle trajectory, $x_p(t)$, is shown in Figure 1. (The trajectory record shown corresponds to data collected for 8 s, at a sampling frequency of 50 Hz, while the entire particle trajectory is monitored for up to 20 h.) To obtain the position data from the radiation signal, a series of data-acquisition and signal-processing steps are employed, which include detector calibration and wavelet-filtering (Degaleesan, 1997). Such topics themselves are worth separate discussions, and thus are beyond the scope of the present article. The studies of Devanathan (1991), Moslemian et al. (1992), Larachi et al. (1994), and Chaouki et al. (1997) provide more detailed information about CARPT for the interested readers. The Lagrangian nature of the CARPT technique, which is the most distinctive feature of CARPT in contrast to the other Eulerian measurements, such as those achieved by PIV and LDA, is clearly manifested. By performing the time differencing of the successive particle positions one obtains the Lagrangian velocity, $\boldsymbol{u}_p(t)$.

The Lagrangian position, $\boldsymbol{x}_p(t)$, and velocities, $\boldsymbol{u}_p(t)$, provide rich and valuable information on the fluid-dynamics and mixing/dispersion properties in a bubble column. Both Lagrangian-type quantities and time-averaged Eulerian-type quantities can be extracted from CARPT data. The turbulent dispersion coefficient tensor, D_{ij}, can be directly calculated as

$$D_{ij}(t) = \frac{1}{2}\frac{d}{dt}\langle x_i x_j \rangle. \qquad (1)$$

Such D_{ij}, as defined in the Lagrangian framework, is closely related to the eddy diffusivity that appears in the convection–diffusion-type conservative equations for any passive scalars in a turbulent flow. For example, in isotropic and homogeneous turbulence it has been shown that the diffusivity appearing in the convection–diffusion equation can be approximated by the Lagrangian-based turbulent-eddy coefficients (Tennekes and Lumley, 1971).

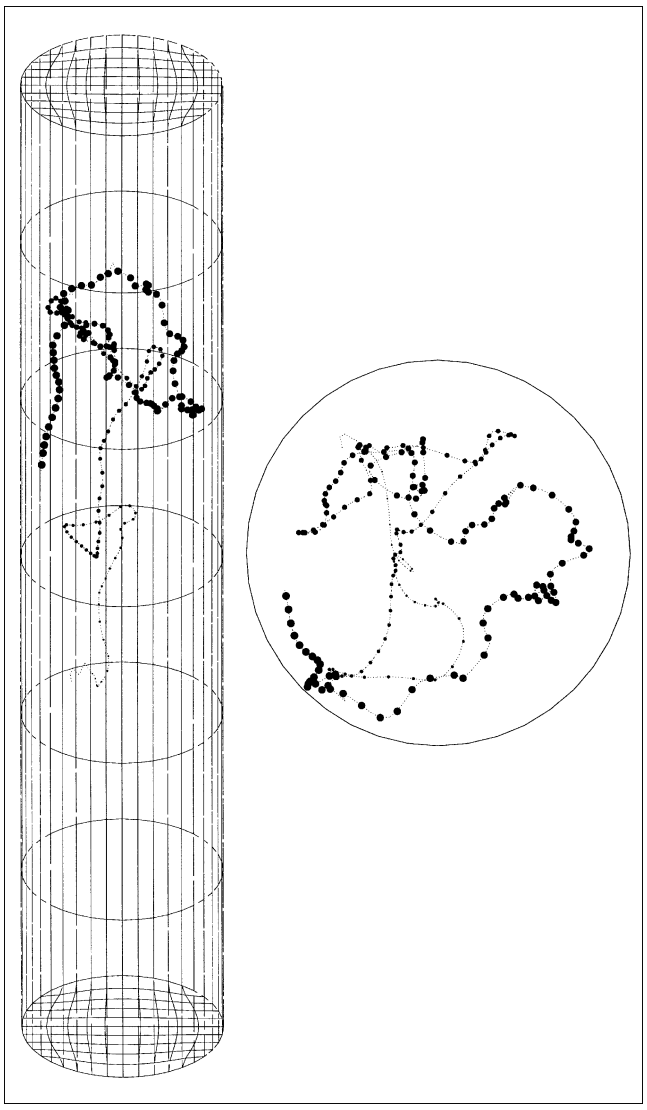

Figure 1. Sample of CARPT experiment for 44-cm column at $U_g = 10$ cm/s.

The diminishing of the circle size indicates the time sequence with the smallest and largest representing the earliest and latest time, respectively. The time interval between the positions is 0.04 s. The total time span is 8 s. The total duration of experiment is up to 20 h.

The time-averaged liquid velocities and turbulence correlations in the Eulerian framework, that is, at different positions in the column, can be calculated from CARPT data provided there is sufficient data to guarantee a convergent statistics. For the purpose of the present objective, which is to determine the nature of the ensemble-averaged quantities resulting from CARPT measurements, a brief description of the data processing involved is provided. The column is divided into compartments. The velocity of the particle is then as-

signed to that compartment that contains the midpoint of the two successive positions of the particle. In this manner instantaneous velocities are assigned to their respective compartments. Ensemble averaging of the velocities in a given compartment is performed over the number of times (repetitions) that the particle visits that compartment. If N is the number of repetitions in a given compartment, the ensemble average liquid velocity component along the ith direction in that compartment is

$$\langle u_i \rangle = \frac{1}{N} \sum_j u_{i,j}, \tag{2}$$

where $u_{i,j}$ is the jth assignment of the ith velocity component to that compartment resulting from the jth visit of the particle. Invoking the ergodic hypothesis, ensemble averaging yields time averaging. Therefore $\langle u_i \rangle$ is taken to be the time-averaged liquid velocity in the given compartment. The turbulence related correlations, $\langle u_i' u_j' \rangle$, are readily calculated after the mean velocities are obtained (Devanathan, 1991; Larachi et al., 1997).

As a Lagrangian measurement technique, CARPT cannot provide the Eulerian type of information for the velocity field, such as $\boldsymbol{u}(\boldsymbol{x}, t)$. A common practice with Eulerian data is to perform a spectral analysis of the velocity field. For an anisotropic and nonhomogenous turbulence, however, since the relation between Lagrangian spectra, which CARPT can

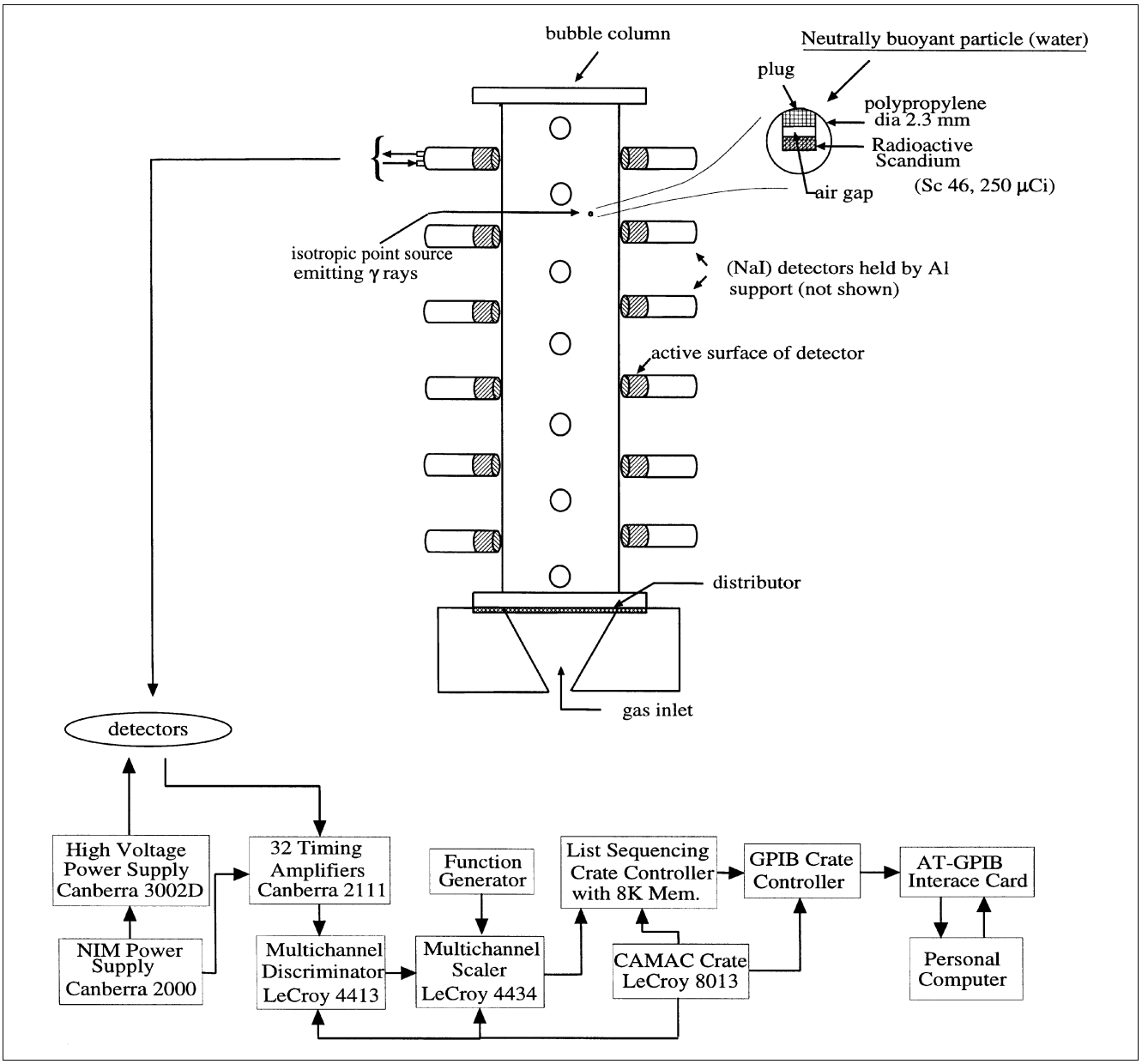

Figure 2. CARPT facility.

provide, and Eulerian spectra, is not straightforward, such analysis would be cumbersome to realize. Nevertheless, we can show that the nature and quantification of the instantaneous flow structures in bubble columns is possible by employing Lagrangian analysis (Cassanello et al., 2001).

The reliability and accuracy of the CARPT measurement largely depends on several key factors, which include the tracer particle, calibration, and signal processing. The issues regarding to the calibration and tracer particle have been discussed in detail by Degaleesan (1997), Kumar et al. (1997a), and Larachi et al. (1997). One of the major issues is how to remove the noise inherently contained in the CARPT raw data. Owing to the quantized nature of the γ photons, the intensity of the radiation emitted by the radioactive tracer particle exhibits continuous fluctuations in time. The instantaneous particle position evaluated from the radiation signal contains such fluctuations. In turn, the Lagrangian velocity of the tracer particle, which is directly calculated from the instantaneous position of the tracer particle via time-differencing, contains spurious velocities. Usually, the noise of this type would result in inaccuracies in the estimation of turbulence-related quantities, such as turbulence intensity and eddy diffusivity, although the mean quantities may not be affected. Since most of the systems where the CARPT technique is applied exhibit highly turbulent natures, such a consequence is obviously undesired. How to remove the noise in the position data of the particle, which causes spurious velocities therefore becomes an important issue in implementation of CARPT technique. Apparently, the calibration cannot eliminate the noise. We proposed a filtering algorithm, based on wavelet analysis, for the removal of intrinsic noise in the instantaneous position data generated by the CARPT measurement. The suitability of such filtering for the CARPT data and its advantage over the conventional filtering technique based on the Fourier transform has been proven and discussed by Degaleesan (1997). The efficiency of the wavelet filtering and its ability to improve the accuracy of measurement are experimentally validated by processing the CARPT data for a particle in controlled motion. It is shown, via processing the numerically generated "chirp" signal, that the method works well for the multifrequency data. Finally, the CARPT data for bubble columns of different size and superficial gas velocity are filtered by the technique. We show that the unfiltered data results in a significant overestimation of turbulence-related quantities and that the wavelet filtering largely reduce such bias. A detailed discussion on this topic is provided by Degaleesan (1997).

Experimental Setup

The bubble column and CARPT setup is shown in Figure 2. In the CARPT technique the detectors are strategically positioned around the column, spanning its entire length. Each detector unit is a cylinder 2.125 in. (54 mm) in diameter and 10.25 ft. (312 cm) long, and contains an active cylindrical NaI scintillation crystal (2 in. by 2 in.). The total number of detectors used is varied depending on the size of the column. Typically 16 (14-cm column) to 26 detectors (44-cm column) were used. With specially designed support structures, the detectors can be held at eight different angular positions with respect to the axis of the column. Each detector is held on

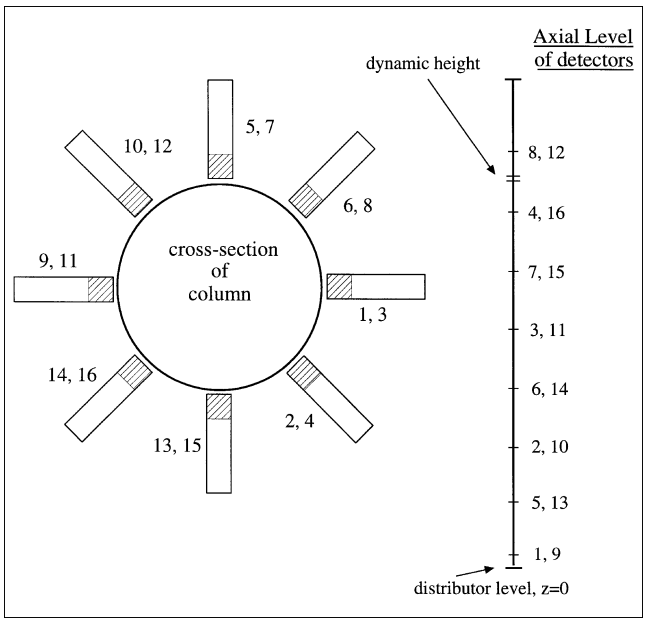

Figure 3. Configuration of detectors in the CARPT experiment.

the support structure such that the axis of the detector is perpendicular to that of the column and the circular face of the detector is tangential to the wall of the column at a given location. The positions of the detectors are measured in cylindrical coordinates. For each detector, with its circular face tangential to the wall of the column, it is thus assured that the axis of the detector is along the radial coordinate of the column. Hence, accurate alignment of the detectors to conform to cylindrical geometry is necessary, since any misalignment leads to error in locating of the particle position. The general configuration of the detectors is shown in Figure 3. Two detectors are positioned at a given axial level, at a 180-degree angle to each other, that is, the two detectors are placed on either side of the column and made to face each other. These two detectors form a pair. At the next higher level, the angular position of the next pair of detectors is increased by 45 deg from that at the level below. Such a configuration ensures equal spacing between all the detectors in all directions. As shown by Larachi et al. (1997), this is the optimum configuration, since it enables the particle always to be close to a set of detectors anywhere in the column, except close to the distributor, below which no detectors were placed.

Scandium-46 (Sc-46) was used as the radioactive source in all the CARPT experiments. Sc-46 has a half-life of 83.5 days and exhibits two photopeaks at 0.889 MeV and 1.13 MeV. In order to make the tracer particle neutrally buoyant, a small Sc ($\rho = 2.99$ g/cm^3) particle is embedded in a polypropylene sphere of outer diameter 2.36 mm, along with a pocket of air, that results in a composite (polypropylene, scandium, and air) sphere that has a density very close (such as 0.9995 to 1.0005 g/cm^3) to that of water, or 1. The method of tracer preparation is similar to that employed by Devanathan (1991). However, in the present method, instead of using a solid cylinder (0.7 mm by 1.0 mm) of Sc, as was done by Devanathan (1991), several smaller particles (about 10 of 100 μm in size) were

embedded in the polypropylene sphere in order to provide more freedom for adjusting the weight, and thereby the density of the tracer particle, which was done by trial and error. Hereafter, "particle" refers to the composite tracer particle (polypropylene, Sc and air).

For all the experiments performed, the density of the particle was adjusted in order to yield a rise velocity of 0.1 to 0.25 cm/s. After some time the particle becomes slightly heavier due to slight water absorption and exhibits almost no rise velocity. Visual observation of the response of the particle to mild agitation in liquid indicated that the particle was able to follow the liquid well.

The sources of error in CARPT are due to the statistical fluctuation of the gamma-ray source and the fluctuation in the density of the medium between the source (tracer particle) and the detectors. Since both fluctuations are Gaussian in nature with deviation of zero mean, all time-averaged CARPT-determined quantities should be unaffected. Questions can be raised, however, regarding cross- and autocorrelations of velocity fluctuations. We have implemented wavelet-based filtering (Degaleesan, 1997) to remove the spurious velocities contributed by gamma source fluctuations and have proved via experiments its success. Nevertheless, because of the finite volume of the tracer particle, and the fact

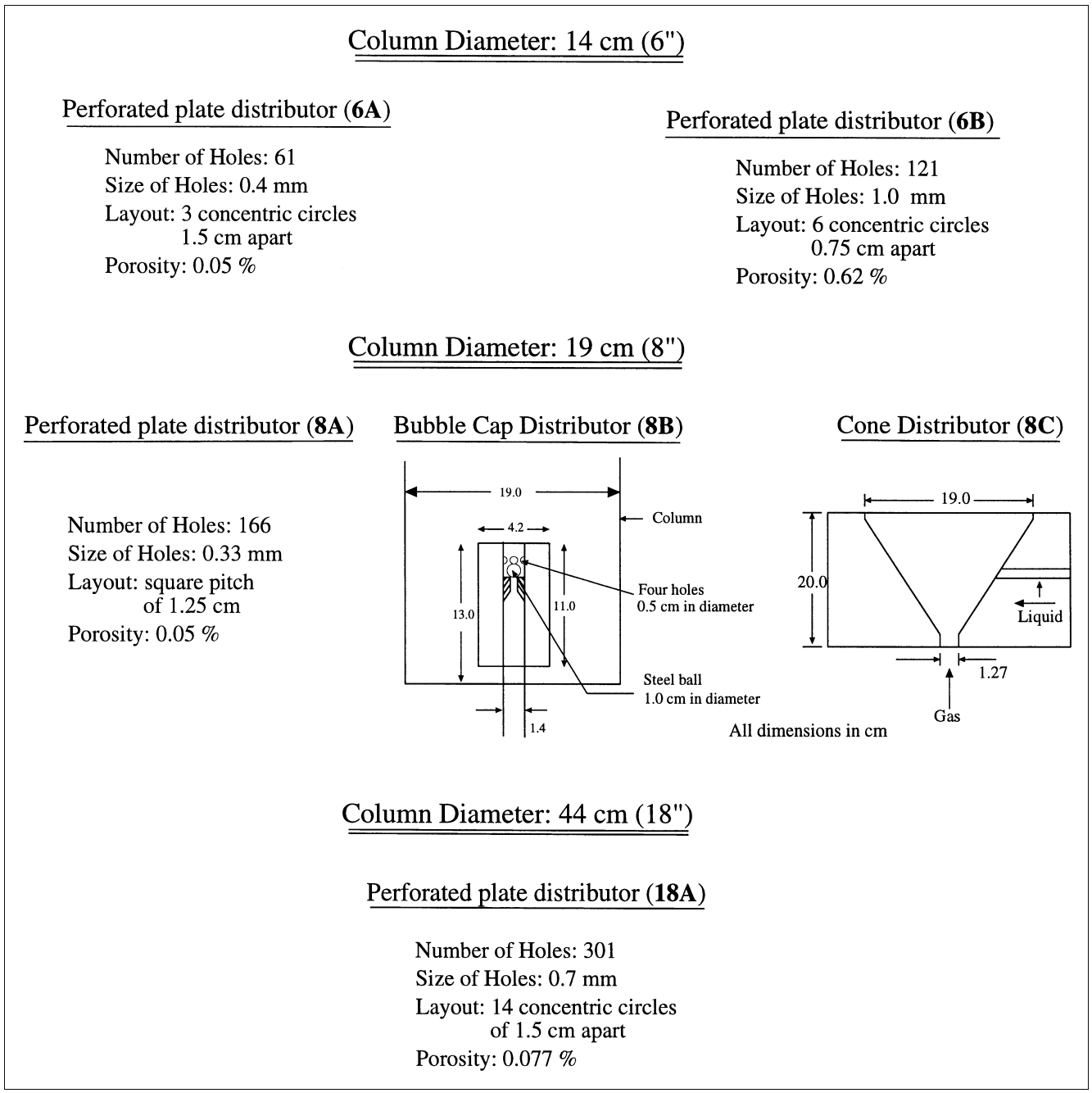

Figure 4. Characteristics of the distributors used.

Table 1. Experimental Conditions

Column Dia. D (cm)	Gas Distrib.	Superficial Gas Vel. U_g (cm/s)	Static Liquid Height (cm)	Dynamic Liquid Height (cm)	Global Gas Holdup $\langle \epsilon \rangle$ %
14	**6A**	2.4	120.2	133.2	9.8
		4.8	98.0	120.4	18.6
		9.6	98.0	126.0	22.2
		12.0	98.0	129.1	24.1
14	6B	2.4	98.0	105.0	6.7
		4.8	98.0	112.0	12.5
		9.6	98.0	123.0	20.3
		12.0	98.0	126.0	22.2
19	8A	2.0	104.0	114.7	9.3
		5.0	103.5	128.0	19.1
		12.0	95.5	124.0	23.0
	8B	12.0	95.5	118.0	19.1
	8C	12.0	95.5	117.0	18.4
44	18A	2.0	179.0	193.1	7.3
		5.0	179.0	209.8	14.7
		12.0	176.1	217.6	19.1

that we assign velocity vectors to the centroids of cells of finite size, it is clear that CARPT, as used at present, cannot provide the fine structure of the flow. We estimate that we can capture any frequencies up to 25–30 Hz, but in large columns our typical spatial resolution of 0.4-cm may not be achieved due to large cell size in data processing. In spite of these deficiencies CARPT provides us with the Lagrangian map of the flow in the entire column and allows estimation of time-averaged flow patterns, as well as of large-scale turbulence structures and their properties.

Operating Conditions

Experiments are performed using air and tap water, under atmospheric conditions. Three columns of internal diameter 14 cm, 19 cm, and 44 cm operated at several different superficial gas velocities were studied. Table 1 lists the column diameter, gas distributor type, and superficial gas velocity; the bed's static and dynamic height; global gas holdup. The data for each CARPT experiment were acquired over a sufficiently large period of time in order to obtain good statistics. The duration of runs for the 14- and 19-cm diameter column is 18 h, and that for the 44-cm-diameter column is 36 h.

Two types of perforated-plate distributors were used in the 14-cm column. The first distributor, referred to as distributor **6A** is similar to the perforated-plate distributor used by Hills (1974), while the second distributor, **6B**, is similar to that of Menzel et al. (1990), who used hot-film anemometer probes to measure the time-averaged velocities and the turbulent Reynolds shear stresses in a 15-cm-diameter column. The objective of using this distributor is to compare the results from CARPT for the Reynolds shear stress $\langle u_r' u_z' \rangle$ with the results of Menzel et al. (1990). The gas superficial velocities for the experiments in the 14-cm-diameter column were chosen to match the operating conditions used by Menzel et al. (1990). The details of the gas distributors are provided in Figure 4.

Experiments in the 19-cm-diameter column, equipped with a perforated-plate distributor **8A**, were conducted at three superficial gas velocities, in the three flow regimes: the homogeneous bubbly flow regime, the transition regime, and the heterogeneous churn-turbulent flow regime. In addition to these experiments, at the highest gas velocity investigated, $U_g = 12$ cm/s, experiments were also conducted using a bubble-cap sparger and a cone distributor. The objective of conducting these additional experiments is to study the effects of distributor on bubble sizes, and thereby on liquid recirculation and turbulence in the churn-turbulent flow regime. CARPT results for the mean liquid velocities in the 19-cm-diameter column with distributor **8A** are also compared with the data from independently conducted heat-pulse anemometer (HPA) experiments.

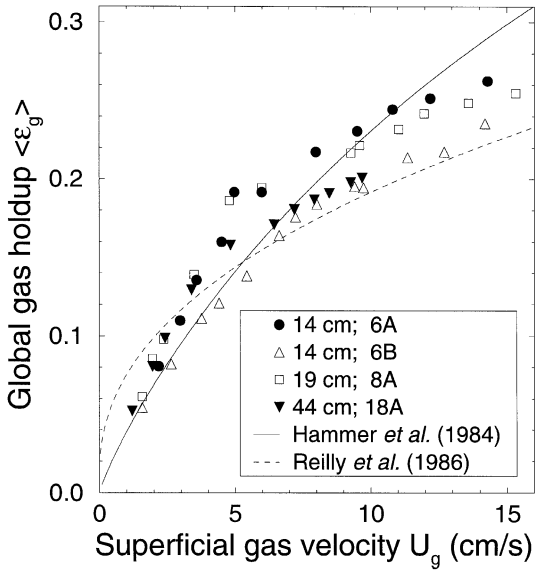

Figure 5. Global gas holdup vs. superficial gas velocity in various columns.

The 44-cm diameter column is the largest column that can be fitted into the current CARPT/CT experimental setup. Experiments in this column were conducted at three gas velocities, similar to the case of the 19-cm-diameter column, using a perforated plate distributor **18A**.

Global gas holdup measurements were made in each column prior to the CARPT experiments, by measuring the bed expansion. The results are presented in Figure 5. A difference is noted between the holdups in the 14-cm-diameter column using the two different distributors. However, these differences diminish with an increase in gas velocity, as is expected (Joshi et al., 1990). No specific trend of the gas holdup with respect to the different column diameters is seen. This is in general agreement with observations in the literature (Joshi et al., 1990). Quantitatively, the correlation of Hammer et al. (1984) and that of Reilly et al. (1986), which are given by Eqs. (3) and (4), respectively,

$$\frac{\langle \epsilon \rangle}{1-\langle \epsilon \rangle} = 0.4\left(\frac{U_g \mu_l}{\sigma}\right)^{0.87}\left(\frac{\mu_l^4 g}{\rho_l \sigma^3}\right)^{-0.27}\left(\frac{\rho_g}{\rho_l}\right)^{0.17} \tag{3}$$

$$\langle \epsilon \rangle = 296 U_g^{0.44} \rho_l^{-0.98} \sigma^{-0.16} \rho_g^{0.19} + 0.009, \tag{4}$$

yield the closest predictions of the observed holdups. In these correlations the sI system of units is used.

A feature that is observed while measuring the global gas holdup is that the gas holdup in the column is sensitive to the static height of the liquid in the column, for a given column diameter. This suggests the axially nonuniform distribution of gas holdup. Kumar (1994) and Kumar et al. (1995b, 1997b) have used computed tomography (CT) measurements of the cross-sectional gas holdup distribution to show that in the middle section (lengthwise) of the column the gas holdup is invariant with axial position. This implies that at the end zones the gas holdup is quite different from in this middle section, and this causes a variation in global holdup measurements with static height. It is expected that for larger column aspect ratios (such as greater than 8) this difference becomes small and eventually disappears, since the contribution of the end zones to the overall gas holdup decreases with an increase in the aspect ratio. In the present study, the L/D ratio was maintained around 7 to 8 for the two columns with the two smaller diameters (14 cm and 19 cm), and around 4.5 for the largest column of 44 cm in diameter.

Time Averaged Liquid Flow Field

With the CARPT technique it is possible to measure the time-averaged flow pattern in the entire flow field. It is of interest to see if there really exists a steady axisymmetric flow pattern in a fully 3-D bubble column. For the purpose of

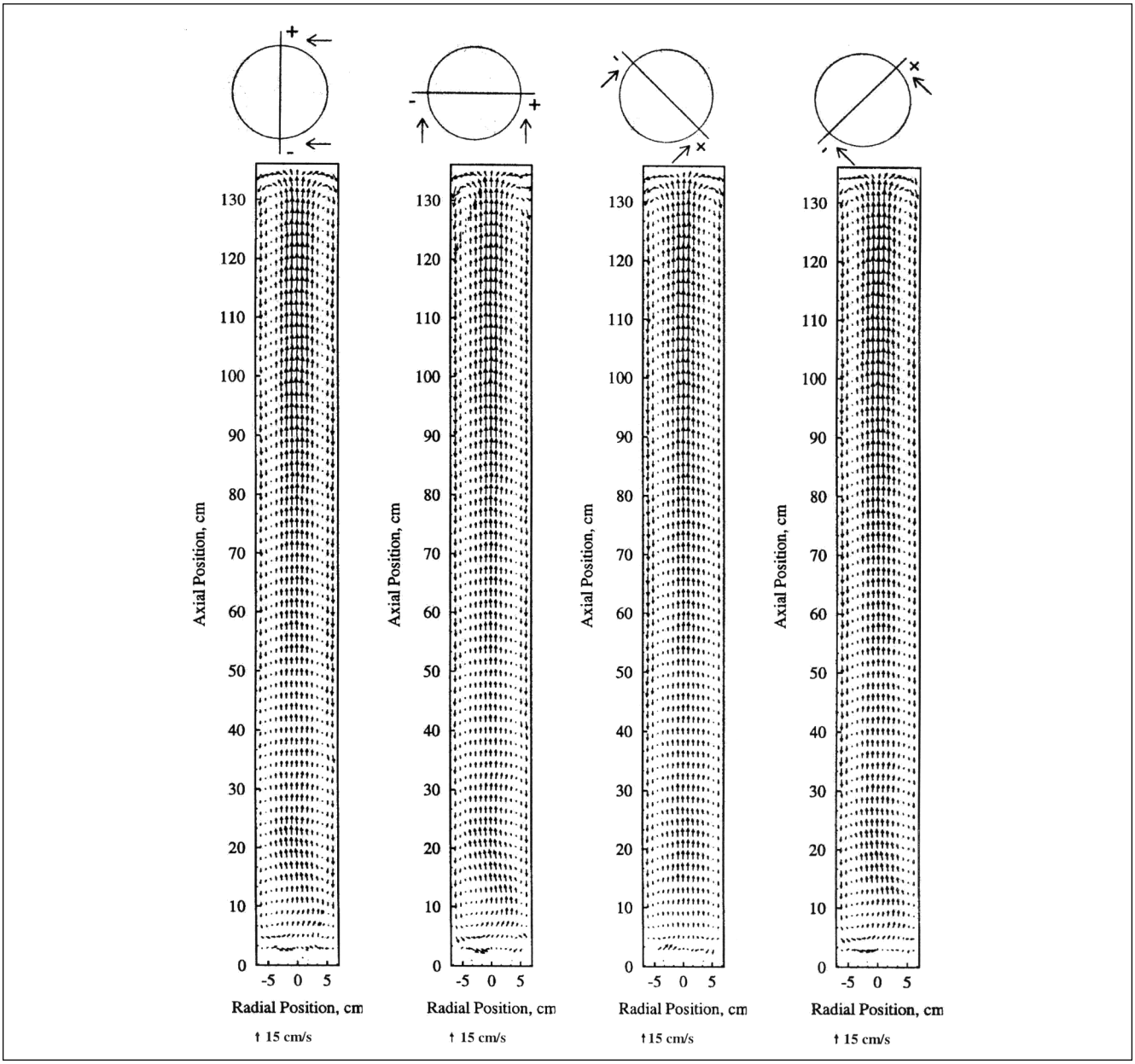

Figure 6. Velocity vector plots (side views) for 14-cm column.

Distributor: perforated plate 6A, $U_g = 2.4$ cm/s; the units of axial and radial location are in cm.

visualization, the domain of the column is sliced with a 2-D plane at different orientations, and vector plots are shown for the time-averaged liquid velocities. Longitudinal (vertical) sections and lateral (cross) sections are presented to interpret all three components of the velocity vectors. The longitudinal plane is made by cutting through the center of the column at an angle. The resulting vector plot shows the corresponding r and z components of the velocities, projected onto the plane. The θ and r components of the velocity can be visualized from the cross-sectional *slice* made at some axial locations in the flow domain.

Figures 6 and 7 show the longitudinal sections and cross sections of the time-averaged velocity vector plots at $U_g = 2.4$ cm/s, in a 14-cm-diameter column, respectively. The angle between the longitudinal planes is $\pi/4$. The choice of these planes is arbitrary. Spanning the entire column, the single-cell circulation flow pattern is clearly seen from various side views, in agreement with the observations of Devanathan (1991). Besides, the flow pattern is reasonably symmetric with respect to the column axis. From a height of about 50 cm above the distributor the flow appears to be quite well developed with negligible radial and angular velocities, as shown in Figure 7c. At the upper end of the column, near the disengagement zone, the flow reversal is symmetric about the column axis resembling a fountain-like pattern, as shown in Figure 7d. At the bottom of the column, shown by Figures 7a and 7b, the time-averaged flow pattern loses its symmetric appearance. In this region the liquid descends predominantly along one side of the column wall and rises along the opposite end. It is important to notice that this asymmetric structure emerges from ensemble averaging of CARPT data, and thus implies that, in the time-averaged sense, there is a preferred direction for the flow near the distributor, which is not symmetric with respect to the column axis.

Visual observation of the flow in the column indicates that the gas bubbles tend to form "swarms" that follow a spiraling motion moving (or rocking) from one side of the wall to the other and gradually seem to get more evenly distributed at higher levels in the column. In a column exposed to strong liquid currents due to liquid recirculation and turbulence, the bubbles are swept about by the liquid currents at the distributor. Even though the spiraling motion does not visually appear to have any preferential direction, it is possible that in a statistical sense, there is indeed a preference that is dictated by some nonuniformity in the distributor, for example, blocking of some of the holes (0.4 mm in diameter for the present case). Permanent blocking of some holes can be caused by chemical deposition due to contaminants present in the water. Therefore, a perfectly uniformly aerated perforated-plate distributor is very difficult if not impossible to achieve for long-term column operation. However, it must be noted that the observed blocked holes are not usually concentrated in one area, but are dispersed over the entire distributor plate. This strong observed asymmetry of the time-averaged flow pattern near the distributor influences the flow behavior above the distributor zone, leading to large downward velocities near one side of the column, where the liquid flows down toward the distributor. These effects slowly disappear with height and the flow becomes symmetric toward the upper section of the column.

Similar flow patterns are observed at higher superficial gas velocities. As expected, the extent of the asymmetry at the distributor is reduced as the gas velocity is increased. For the experiments using the distributor **6B** in the 14-cm-diameter column, the distinct asymmetry near the distributor is not observed for any gas velocities, including the lowest gas velocity of 2.4 cm/s. This may be due to the fact that the holes on plate **6B** are more uniformly distributed and its overall porosity is much larger (about 10 times) than that of **6A**.

In larger columns at high U_g the single-cell circulation pattern is still observed, as shown by Figure 8. The presence of the asymmetric sheetlike structure close to the distributor can also be seen as shown by Figure 9. It appears that far above the distributor, that is, at about 3.0 times the column diameter (132 cm), the flow becomes symmetric about the column axis. Notice that the aspect ratio of the column, that is, 4.5, is relatively low.

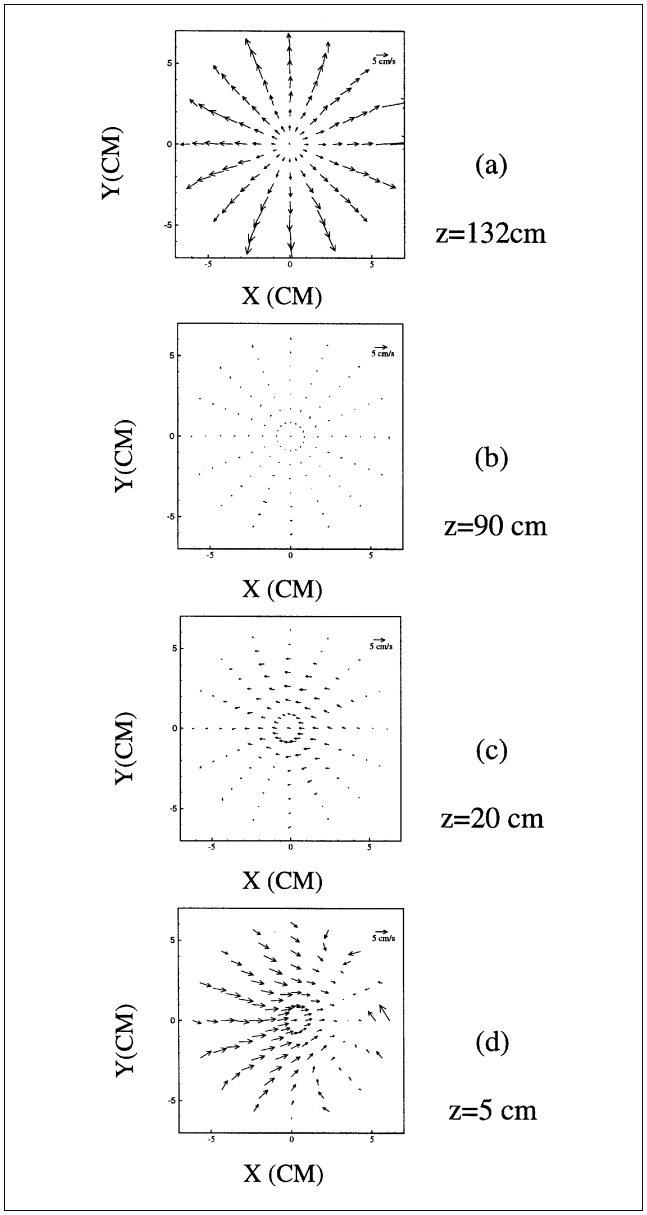

Figure 7. Velocity vector plots (cross-sectional views) for 14-cm column.

Distributor: perforated plate 6A; $U_g = 2.4$ cm/s.

The preceding results, based on a 3-D interpretation of the time-averaged flow field, show that there is a statistically stationary flow pattern in bubble columns, away from the end zones (distributor and disengagement zone) where a time-averaged recirculating velocity profile is seen. The general observation is that in this region the ensemble-averaged axial liquid velocities dominate (15 cm/s to 60 cm/s), and the averaged radial and angular velocities are negligible (≤ 1 cm/s), and can be considered to be zero. For the columns with large aspect ratio (≥ 7), symmetry exists with respect to the column axis in this region. Near the distributor zone, however, a symmetric flow pattern about the column axis is absent. The extent of asymmetry seems to depend on the distributor used. The asymmetry in the time-averaged flow in this region is therefore attributed to the influence of the distributor. For most cases in the well-developed middle region of the column, the axial variation of the time-averaged velocities is not significant. For all the columns operated at all the superficial gas velocities, there is no evidence of multiple circulation cells in the time-averaged sense.

It should be noted that the ability of CARPT to obtain time-averaged liquid velocities has been compared with results obtained by independent techniques. At low gas holdups, where PIV can be considered the state-of-the-art standard, very good agreement between CARPT and PIV was obtained (Chen et al., 1999). Some of the observed discrepancies were due to the different quality of water in St. Louis and Columbus and the inability of PIV to get data at higher gas velocities. The validity of CARPT-determined mean flow structures flow was confirmed.

Mean Axial Liquid Velocity and Reynolds Shear Stress

The flow of gas–liquid mixture in bubble columns can be described by the two-fluid model (Drew, 1983), in which both

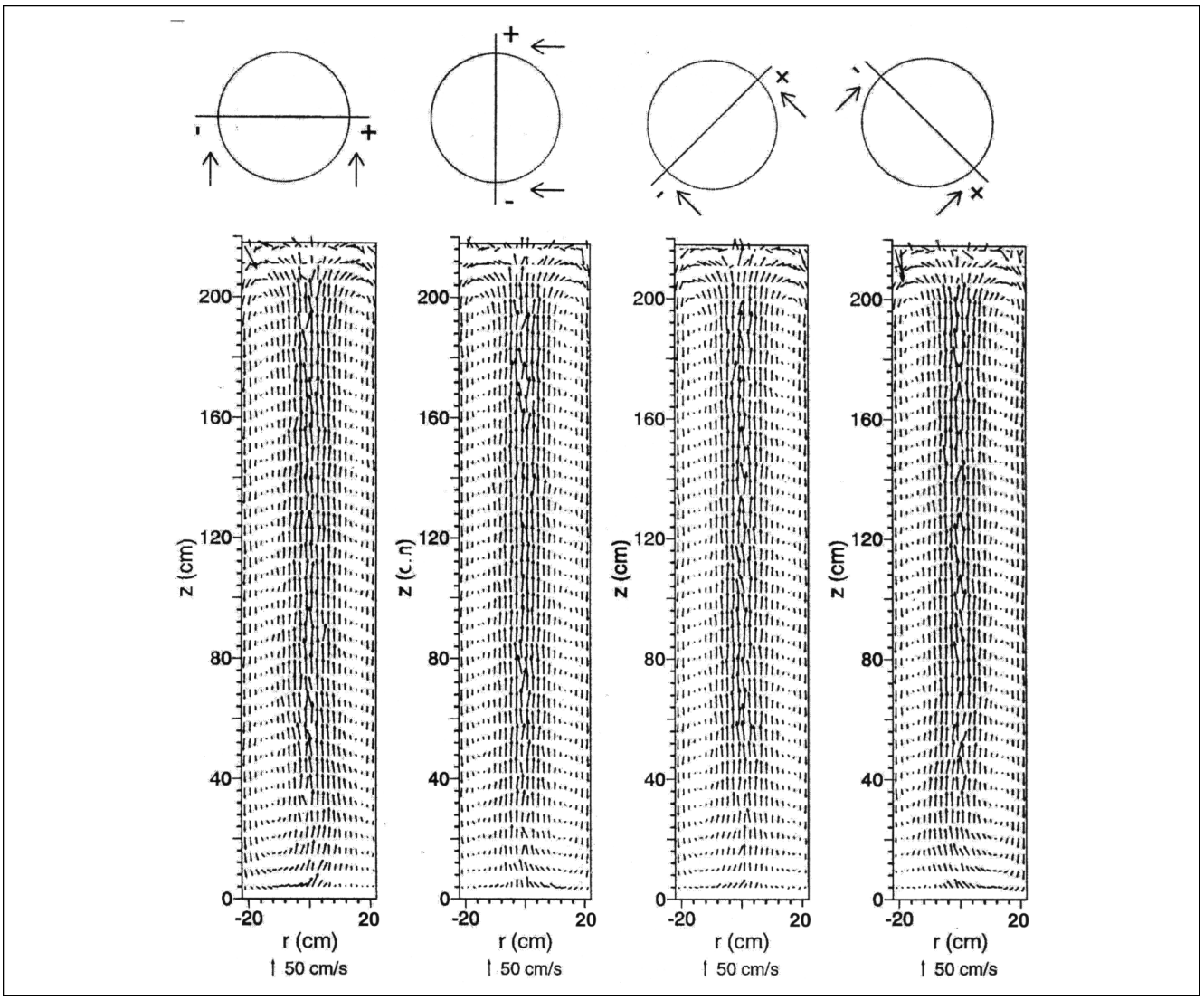

Figure 8. Velocity vector plots (side views) for 44-cm column.

Distributor: perforated plate **18A**; $U_g = 10$ cm/s.

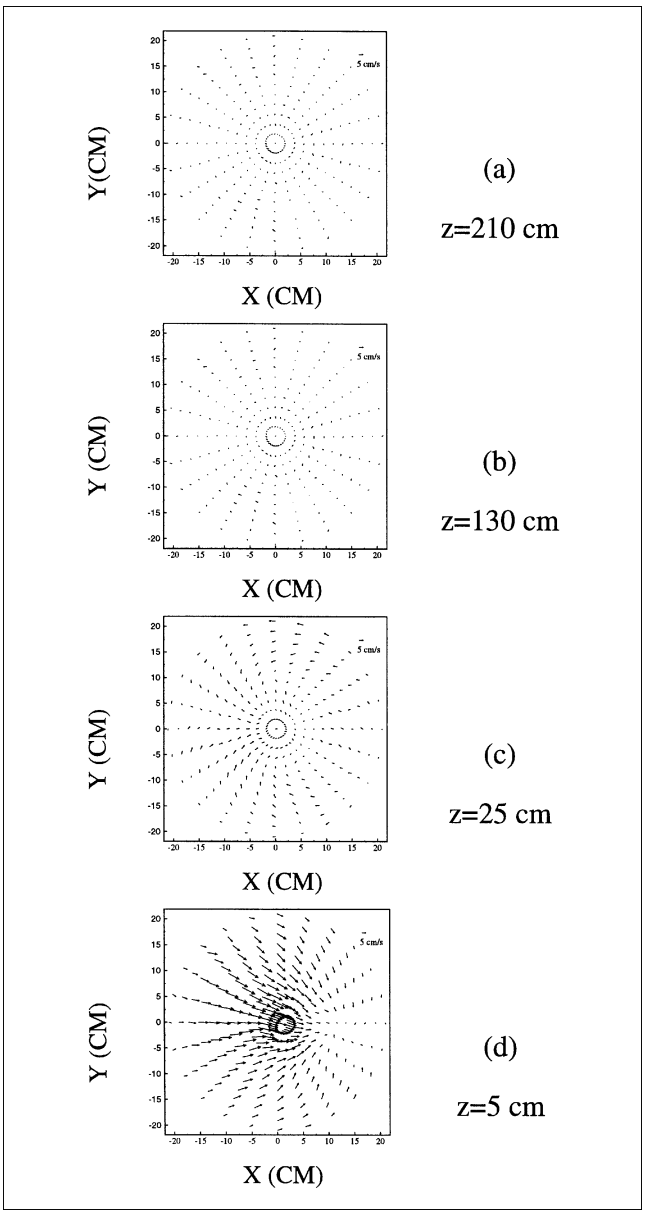

Figure 9. Velocity vector plots (cross-sectional views) for 44-cm column.

Distributor: perforated plate **18A**; $U_g = 10$ cm/s.

the liquid and gas phase are treated as continuous, interpenetrating media, and the motion of each phase is thus governed by an Eulerian type of equation. A 1-D model for liquid recirculation in bubble columns is the simplified form of the two-fluid model. In such a model the flow is assumed to be, in the sense of time-averaging, steady, fully developed, axisymmetric, and the end effects are considered negligible. In the cylindrical coordinate system, it is written as

$$\frac{1}{r}\frac{d}{dr}\left[r(1-\langle\epsilon\rangle)\tau_t\right]-\frac{dP}{dz}-\rho_l[1-\langle\epsilon\rangle]g=0, \qquad (5)$$

where, $\tau_t(=-\rho_l\langle u'_r u'_z\rangle)$, represents the Reynolds shear stress. The pressure gradient is related to the global gas holdup, $\langle\epsilon\rangle$, and wall shear stress, τ_w, through the global momentum balance for fully developed flow:

$$-\frac{dP}{dz}=-\frac{2\tau_w}{R}+\rho_l(1-\langle\epsilon\rangle)g. \qquad (6)$$

The existence of such steady 1-D liquid profiles is supported by the experimental evidence (Menzel et al., 1990; Devanathan, 1991), including the present results that are shown in the previous section. Solution of Eq. 5 requires the gas holdup profile, $\epsilon(r)$, and a closure for the Reynolds shear stress, τ_t. The most advanced noninvasive technique for measuring the gas holdup in gas–liquid systems is the CT technique (Kumar et al., 1995b, 1997b). Several attempts have been made (Ueyama and Miyauchi, 1990; Lou and Sevendsen, 1991; Geary and Rice, 1992; Kumar et al., 1994, 1995b), to develop 1-D models for liquid recirculation. At present, a closure for the Reynolds shear stress can only be developed from the experimental data. However, such data from direct measurements are very limited. Menzel et al. (1990) used the HPA technique to measure the correlation $\langle u'_r u'_z\rangle$ in columns of two different sizes at several gas superficial velocities. Devanathan et al. (1990) provided some preliminary results of the Reynolds stress profile obtained from CARPT experiments. Using the PIV technique, Mudde et al. (1997) measured the Reynolds stress distribution in 2-D bubble columns. This measurement, however, is limited to the situations of low gas superficial velocity and is 2-D due to the nature of the PIV technique. For the purpose of developing the 1-D model, there is a need for experimental data of Reynolds stress and mean liquid-velocity profiles for bubble columns of different sizes and operated over a range of superficial gas velocities. One of the major objectives of the present study is to provide such a database.

In general, liquid recirculation is dependent on a number of process parameters: superficial gas velocity, column size,

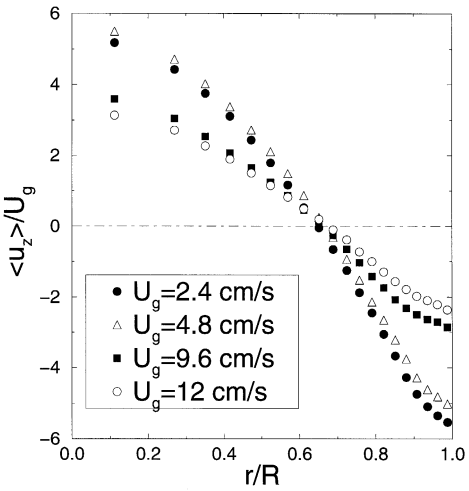

Figure 10. Nondimensional time-averaged axial liquid velocity profiles in the 14-cm column with perforated plate 6A as gas distributor operated at different superficial gas velocities.

The axial averaging range: $0.15H_D \le z \le 0.85H_D$. H_D is column's dynamic height.

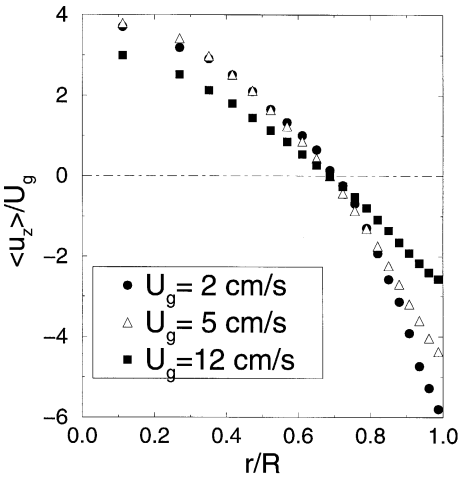

Figure 11. Time-averaged nondimensional axial liquid velocity profiles in the 19-cm column with perforated plate 8A gas distributor operated at different superficial gas velocities.

The axial averaging range: $0.15H_D \le z \le 0.85\ H_D$. H_D is column's dynamic height.

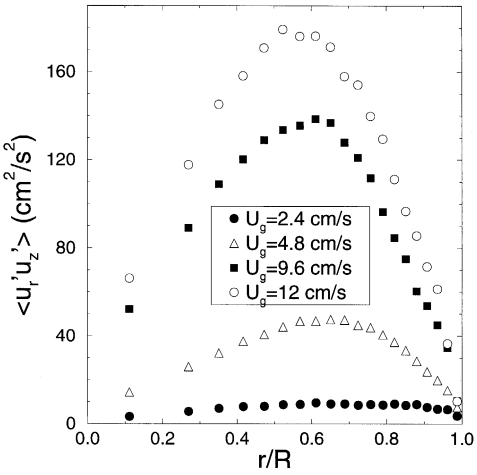

Figure 13. One-dimensional Reynolds stress distribution in the 14-cm column, with perforated plate 6A gas distributor, operated at different superficial gas velocities.

The axial averaging range: $0.15H_D \le z \le 0.85H_D$. H_D is column's dynamic height.

physical properties of liquid and gas, gas sparger type, and so forth. Among these, the superficial gas velocity, U_g, and column diameter, D, are the two key parameters that dominate the fluid dynamics of a bubble column. For the purpose of scale-up and design of bubble columns, one needs a 1-D liquid recirculation model in nondimensional form. The column diameter and superficial gas velocity therefore become the natural candidates for the characteristic integral length scale and velocity scale. Figures 10, 11, and 12 show the profiles of the time-averaged nondimensional mean axial liquid velocity, that is, $\langle u_z \rangle / U_g$ as a function of r/R, for three columns of different size and operated at different superficial gas velocity. From Figure 10, one immediately sees that the curves fall into two groups: one for U_g of 2.4 cm/s and 4.8 cm/s, and the other for U_g of 9.6 cm/s and 12 cm/s, which clearly represent the bubbly flow regime and churn turbulent flow regime, respectively. The fact that the nondimensional profiles for the same flow regime overlap indicates that different similarity solutions can exist for the different flow regimes. The fact that the nondimensional liquid velocities of the turbulent flow group, that is, U_g of 9.6 and 12 cm/s, are smaller than those of the bubbly flow group, that is, U_g of 2.4 and 4.8 cm/s, indicates that as flow transits from bubbly to churn turbulent the dependence of liquid velocity on the superficial gas velocity, which is nearly linear in bubbly flow, changes. A similar trend is observed in the 19-cm column, as shown by Figure 11. However the liquid mean velocity profiles for the 44-cm column do not overlap after such scaling, as shown by Figure 12.

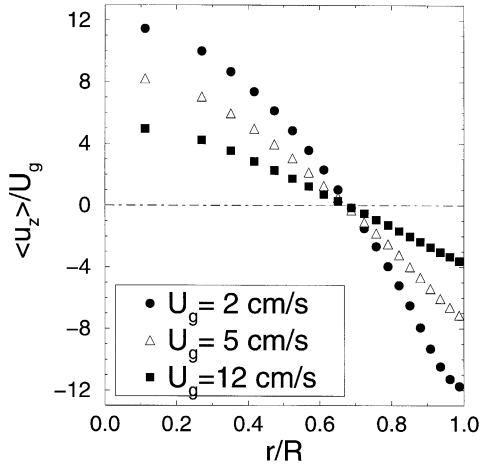

Figure 12. Time-averaged nondimensional axial liquid velocity profiles in the 44-cm column with perforated plate 18A gas distributor operated at different superficial gas velocities.

The axial averaging range: $0.15H_D \le z \le 0.85H_D$. H_D is column's dynamic height.

The Reynolds shear stresses, $\langle u_r' u_z' \rangle$, calculated from the CARPT experiments, are plotted as a function of superficial gas velocity for various column sizes in Figures 13, 14, and 15. The behavior of the shear stress is very similar to that of single-phase turbulent flow in a circular pipe. The large changes in the values of $\langle u_r'\ u_z' \rangle$ indicate the transition from the bubbly flow regime to the churn turbulent flow regime. The radial variation of the shear stresses seems to be similar in general shape for all the cases, showing a maximum close to the position of flow inversion. Such profiles are compatible with the parabolic shape of the mean axial velocity as displayed in Figures 10, 11, and 12, as they are consistent with the 1-D model, Eq. 13. The nonzero, positive $\langle u_r'\ u_z' \rangle$ can be interpreted in two different ways. In terms of a correlation, this implies that for a positive perturbation in the axial direction, the system reacts by a positive displacement in the radial position. Physically, this means that the vortices or eddies have a preference to a $(+z, +r)$ rotation. From a

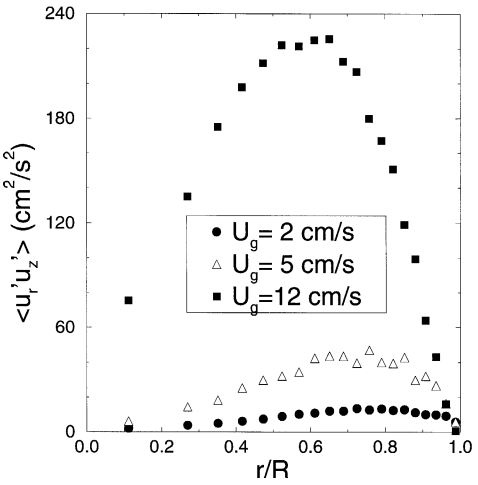

Figure 14. One-dimensional Reynolds stress profile in the 19-cm column, with perforated plate 8A gas distributor, operated at different superficial gas velocities.

The axial averaging range: $0.15H_D \le z \le 0.85H_D$. H_D is column's dynamic height.

shear-stress point of view the positive $\langle u'_r u'_z \rangle$ means that a shear in the axial velocity causes an outward radial transport of momentum. The transition from bubbly flow to churn turbulent flow is clearly observed in the 14- and 19-cm columns, while it is not so obvious for the 44-cm column. In fact, this is consistent with the mean velocity profiles shown in Figures 10, 11, and 12.

One common and distinct feature for all column diameters and superficial gas velocities is that the inversion point for the ensemble-averaged liquid axial velocity is always located at $r/R \approx 0.65$. The inversion point of the ensemble-averaged axial liquid velocity roughly corresponds to the location of the maximum absolute value of the Reynolds shear stress, that is, $\langle u'_r u'_z \rangle$. At this point, in the sense of time averaging, the liquid flow is, in fact, countercurrent. The high Reynolds shear stress around the inversion point may be caused by strong bubble interactions in this zone. It has been observed in the experiments that large bubbles drive the liquid moving up in the core region of the column while small bubbles are carried downwards by the liquid, particularly in the churn turbulent flow regime. The zone where large bubbles regularly meet small bubbles with opposite direction of motion to each other is therefore located around the inversion point. Strong bubble–bubble interactions, that is, bubble coalescence and breakup, occur in this region. Such interactions could result in an enhancement of turbulence shear stress.

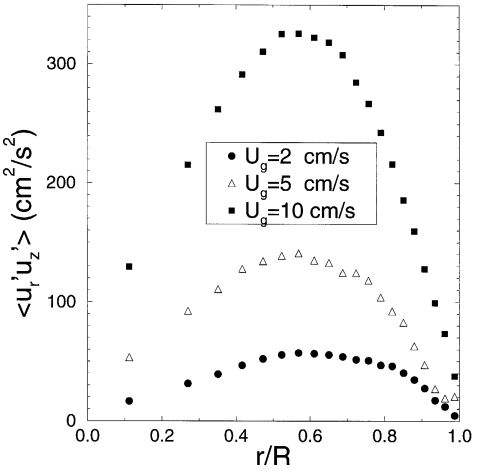

Figure 15. One-dimensional Reynolds stress profile in the 44-cm column, with perforated plate 18A gas distributor, operated at different superficial gas velocities.

The axial averaging range: $0.15H_D \le z \le 0.85H_D$. H_D is column's dynamic height.

Turbulent Velocity Correlations

Modeling a turbulent flow by means of the average Reynolds equations gives rise to the second-order correlations, $\langle u'_i u'_j \rangle$, of the velocity fluctuations. In cylindrical coordinates, the autocorrelations, $\langle u'_z u'_z \rangle$, $\langle u'_r u'_r \rangle$, and $\langle u'_\theta u'_\theta \rangle$, are conventionally called turbulence intensities. Hence, the summation of the three autocorrelations simply gives the turbulent kinetic energy. The cross-correlations, $\langle u'_r u'_z \rangle$, $\langle u'_z u'_\theta \rangle$, and $\langle u'_z u'_\theta \rangle$ represent the turbulent shear stress. From the 1-D model, Eq. 13, one can see that only the Reynolds shear stress, $\langle u'_r u'_z \rangle$, contributes to the axial mean momentum. However, the characteristics of liquid-phase turbulence are revealed at the first level by all of these correlations.

Experimental evidence (Franz et al., 1984; Devanathan et al., 1990; Chen et al., 1994; Mudde et al., 1997) indicates that turbulence in bubble columns is not isotropic. The fluctuations in the axial direction are much stronger than in the radial and angular directions. Visual observation of the flow, especially at high superficial gas velocity, indicates the presence of large-scale spiral structures that are generated by the passage of the gas bubbles and the subsequent bubble–wake interaction. Such spiral structures, whose primary axes are inclined toward the column axis, are spontaneous and intermittent. Since there is lesser restriction in the axial direction to the path of these structures, the length scales in the axial direction are significantly larger than in the radial direction, which is restricted by the diameter of the column. The diameter of the column also restricts the tangential velocities and therefore the azimuthal length scales.

As a typical example, Figure 16 shows the axially and azimuthally averaged radial profiles of all six components of the turbulent velocity correlation tensor, $\langle u'_i u'_j \rangle$, in a 44-cm column operated at $U_g = 10$ cm/s. The turbulence intensity in the axial direction is much higher (by about a factor of 2) than the ones for the radial and azimuthal directions, and thus $\langle u'_z u'_z \rangle$ dominates the turbulent kinetic energy. The shear stresses, $\langle u'_r u'_\theta \rangle$ and $\langle u'_z u'_\theta \rangle$, are actually negligible in comparison with Reynolds shear stress $\langle u'_r u'_z \rangle$ and can be considered to be zero. This implies that the rotational movement of the spiraling vortex structures is uncorrelated from its axial and radial movement. This also means that there is no net transport of axial or radial momentum in the azimuthal direction. The azimuthal and radial turbulence in-

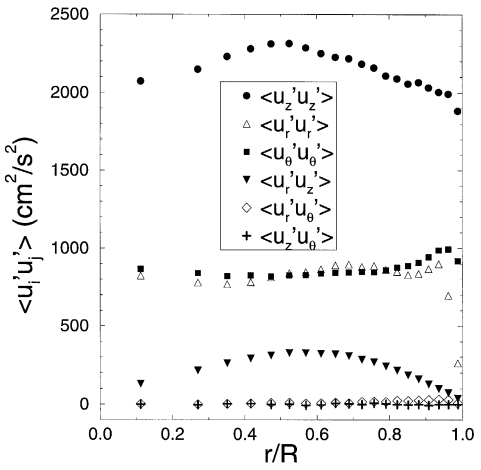

Figure 16. Turbulence intensities in a 44-cm column at $U_g = 10$ cm/s; gas distributor 18A.

The axial averaging range: $0.15H_D \le z \le 0.85H_D$. H_D is column's dynamic height.

tensities are about the same order of magnitude in most of the column. The steep drop of the $\langle u'_r u'_r \rangle$ profile as $r/R \to 1$ is obviously due to the suppression of wall–normal velocity fluctuations by the presence of a nonpenetrating solid wall.

Perhaps the most noteworthy feature of the turbulence intensity distributions for the gas-driven liquid flows, in contrast to that for the pressure-driven liquid (single-phase) flow (Kim et al., 1987; Kreplin and Eckelmann, 1979), is their nondiminishing trend toward the center of the column. The profiles of $\langle u'_r u'_r \rangle$ and $\langle u'_\theta u'_\theta \rangle$ are noticeably flat across the column except for the near wall region. This feature is clearly due to the large-scale vortical spiral structures that spiral up along, and spontaneously cross over the column axis. The relatively constant value of $\langle u'_\theta u'_\theta \rangle$ as $r \to 0$, implies that the angular velocity of this spiral motion about the column axis is intensified when it moves toward the center. This behavior of the eddies and vortical structures rules out the possibility of performing a transient simulation of flows in bubble columns using 2-D axisymmetric codes, since, under these circumstances, imposing a zero gradient at the center line is not realistic and will contradict the existing physical evidence of the nature of the flow. In addition, the transient 3-D vortical structures cannot be captured in a 2-D axisymmetric simulation due to the absence of the θ-dimension.

Expecting an enhancement in turbulence as the superficial gas velocity increases, in Figure 17 we plot the profiles of turbulent intensities for the 14-cm-diameter column operated at different U_g. A distinct feature, particularly for high superficial gas velocities, is that $\langle u'_r u'_r \rangle$ peaks at the center of the column. It may be caused by the strong swing of the spiral structures crossing the center of the column. Recalling the Reynolds stress distributions shown in Figure 13, such swing motions are not correlated with the axial fluctuation.

The profiles of axial turbulence intensity, $\langle u'_z u'_z \rangle$, vary with superficial gas velocity. At low gas velocities, these profiles tend to peak near the column wall. With a further increase in gas velocity, this peak seems to shift more toward the middle of the column radius. At relatively low gas velocity, observations indicate that instantaneous flow has a central upward

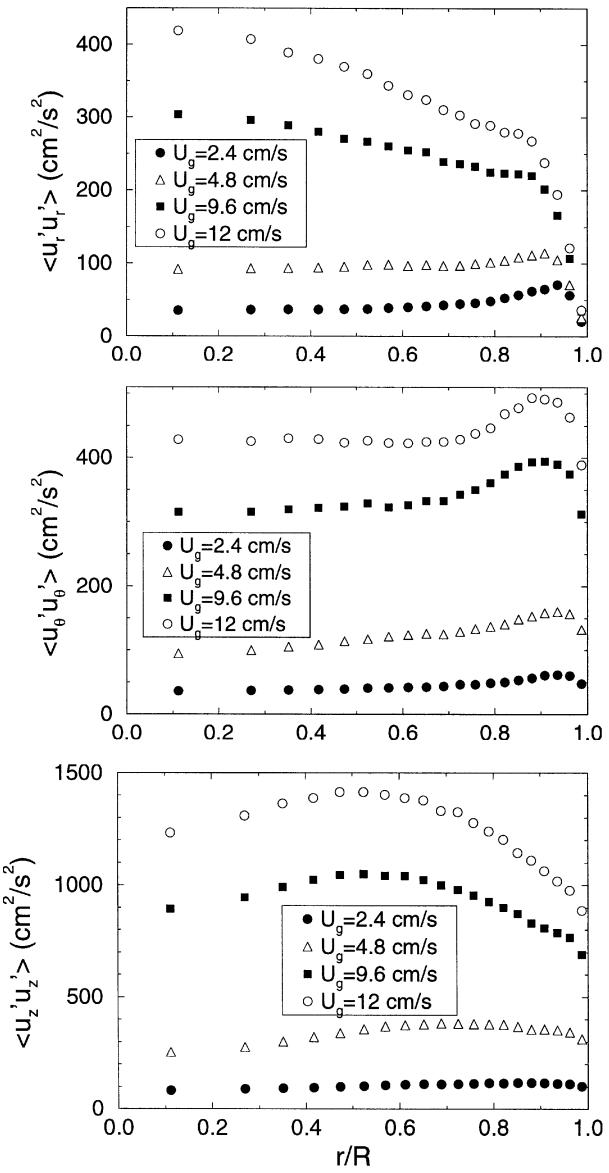

Figure 17. Turbulence intensities in 14-cm column at different U_g.

Gas distributor: **6A**. The axial averaging range: $0.15H_D \le z \le 0.85H_D$. H_D is column's dynamic height.

spiraling motion of the gas plume, which rocks laterally back and forth. The down-flowing liquid between the central bubble stream and the wall is also characterized by liquid vortices that contribute to the large fluctuations in the velocities, in all directions. With an increase in gas superficial velocity, there is an increase in gas holdup and a more intense coalescence of the bubbles with the formation of larger bubbles or gas "pockets" that rise discretely up the column in spiraling paths of constantly changing diameter. Hence, while an increase in superficial gas velocity causes an increase in the overall magnitude of the velocity fluctuations, it also tends to spread the fluctuations over the column cross section. As a result, the profiles for the axial normal stresses start to peak increasingly toward the middle annular region rather than at the wall of the column.

It should be noted here that due to the finite size of the tracer particle used in the CARPT experiments, the maximum range of frequencies tracked by the particle are up to 30 Hz. Therefore the present measurements represent only the large scales of the turbulence structures. However, since the large scales contain the most energy, it is expected that what remains due to the smaller scales is not very significant in magnitude.

Effect of Gas Distributor

Experiments were performed to investigate the effect of distributor on the fluid dynamics in the 14- and 19-cm-diameter columns equipped with various types of gas distributors. For the 14-cm-diameter column, the perforated plate **6B** was used at the same superficial gas velocities employed with distributor **6A**. For 19-cm column, the perforated plate **8A**, bubble cap **8B**, and inverted cone **8C** were used as gas distributors. For a given column and gas superficial velocity, a change in the distributor directly affects the bubble size at formation and the initial distribution of bubbles in the system, which in turn affects the fluid dynamics. In order to analyze the effects of distributors, and thereby bubble size, on the hydrodynamics of the system, the present article considers the ensemble-averaged axial liquid velocity and Reynolds shear stress, which are representative quantities of the fluid dynamics.

Figures 18 and 19 show profiles of $\langle u_z \rangle$ and $\langle u_r' u_z' \rangle$, respectively, in the 14-cm-diameter column using **6A** and **6B**. As shown in Figure 4, the perforated plate **6B** generates larger bubbles and more uniform gas input than **6A**. In the bubbly flow regime at $U_g = 2.4$ cm/s, since the bubbles tend to rise in a rather rectilinear manner, a larger bubble size yields larger rise velocities and thereby higher liquid recirculation velocities. At higher gas velocities, in the transition and churn turbulent flow regime, the trends are the opposite: the liquid velocity for **6A** is higher than that for **6B**. Since **6A** generates smaller bubbles than **6B**, the total momentum input rate from the former is larger than that from the latter, which in turn results in larger liquid recirculation velocity. Such reasoning is valid provided that the gas-volume fractions are the same for both. However, the gas holdups for **6A** and **6B** at the same U_g of high value are significantly different, as shown in Figure 5. A direct comparison therefore cannot be made. The difference in Reynolds stress, on the other hand, diminishes as U_g increases.

At the same superficial gas velocity, the column with the bubble-cap distributor and cone distributor obviously results in larger initial bubble sizes and thus a more concentrated momentum source than for those with the perforated-plate distributor. The flow appeared more violent for the case of the cone and the bubble cap, with large structures frequently moving up the system in a spiraling motion. With the perforated plate, on the other hand, the flow appeared less violent and the large structures were less distinct and frequent.

Figure 20 shows a comparison of the ensemble-averaged axial liquid velocity measured in the 19-cm-diameter column

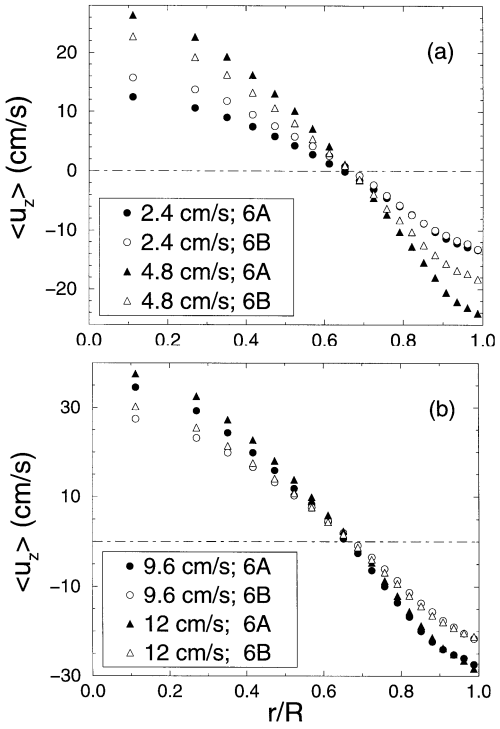

Figure 18. Axial liquid velocity profiles of 14-cm column using perforated plates 6A and 6B as gas distributors, operated at different superficial gas velocities.

The axial averaging range: $0.15H_D \le z \le 0.85H_D$. H_D is column's dynamic height.

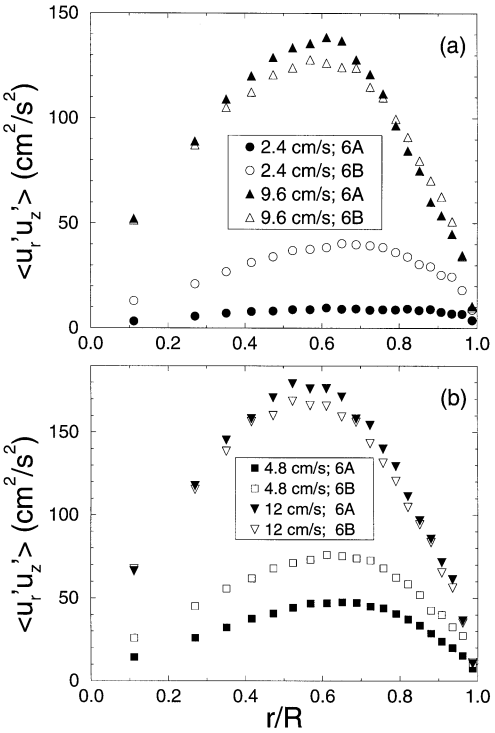

Figure 19. Reynolds shear stress, $\langle u_r' u_z' \rangle$, for 14-cm column using perforated plates 6A and 6B as gas distributors, operated at different superficial gas velocities.

The axial averaging range: $0.15H_D \le z \le 0.85H_D$. H_D is column's dynamic height.

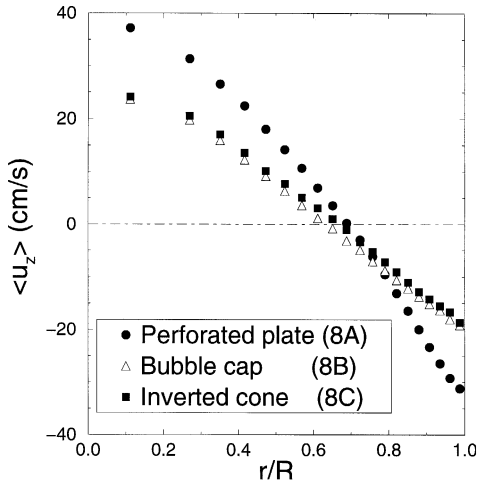

Figure 20. Time-averaged axial liquid velocity profiles in the 19-cm column with different gas distributors operated at superficial gas velocity U_g = 12 cm/s.

The axial averaging range: $0.15H_D \le z \le 0.85H_D$. H_D is column's dynamic height.

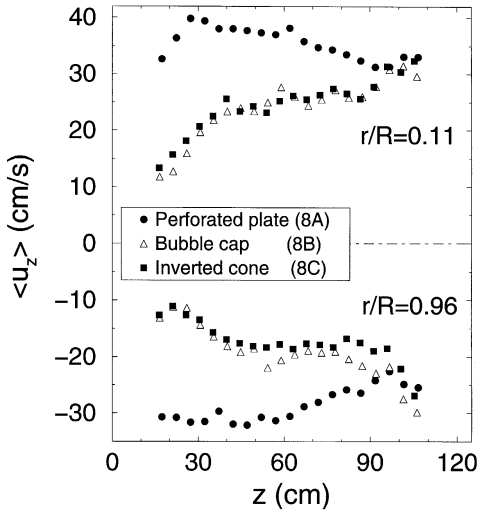

Figure 22. Time-averaged liquid axial velocity along the axial location in the 19-cm column with different gas distributors operated at superficial gas velocity U_g = 12 cm/s.

The velocities are taken at two radial positions. One is in the center region: $r/R = 0.11$; the other in the wall region: $r/R = 0.96$.

using different distributors, at the superficial gas velocity of 12 cm/s. The trends imply that for bubbles of initially larger size, which are generated from the cone and bubble cap, the time-averaged axial liquid velocity gets suppressed in comparison with that for the relatively smaller bubble sizes. The profiles of Reynolds stress are shown in Figure 21. Again the ones for the cone and bubble-cap distributor are identical and their difference from that of the perforated plate is significant in the intermediate range of the radial position. Since the primary differences between the different gas distributors are the initial bubble size and bubble velocity, their effects on the liquid velocities would be most significant in the region close to the bottom of the column and diminish in the upper part of the column. In fact, due to bubble coalescence/breakup and redispersion, one would expect that the average bubble size in the column eventually reaches some intermediate value. One way to examine such effects is to look at the axial variation of the liquid velocities. Figure 22 shows the time-averaged axial liquid velocity variations along the column axis, close to the column center and close to the wall, respectively. Initially the perforated plate generates small bubbles with high injecting velocity, which in turn gives higher momentum per unit volume than that generated by low-speed large bubbles that are injected from the bubble cap and the cone. Notice that the overall gas holdup for distributor **8A** is about 20–25% higher than holdups generated by **8B** and **8C**, as shown in Table 1. We know that the gas holdup profiles at high gas superficial velocity exhibit parabolic-like shape with the peak located at the center of the column (Kumar et al., 1997b). Besides, the interphase momentum exchange per unit volume is proportional to the local gas holdup and is inversely proportional to the bubble size. For these reasons, in the center region, where the liquid is driven by bubbles, liquid velocity for **8A** is much higher than those for **8B** and **8C**, as shown in the upper part of Figure 22. In the wall region, where gas holdup is low, the downward liquid flow is primarily determined by the recirculation that obeys the mass balance. In comparison with that for **8B** and **8C**, the high downward velocity for **8A** is therefore consistent with the high upward velocity in the core region, as can be seen by comparing the lower and upper parts of Figure 22. As expected, such differences become smaller as one moves up the column. Notice that the radial profiles of the liquid axial velocity, shown in Figure 20, are based on the spatial averaging over the middle part of the column, that is, from $z = 30$ to $z = 90$ for this particular case. While the axial

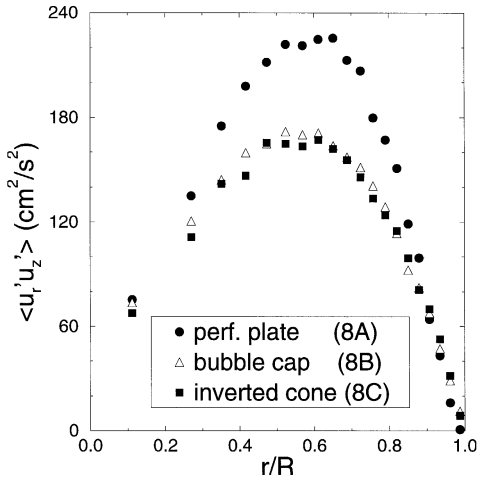

Figure 21. Reynolds stress of 19-cm column with different gas distributors operated at superficial gas velocity U_g = 12 cm/s.

The axial averaging range: $0.15H_D \le z \le 0.85H_D$. H_D is column's dynamic height.

liquid velocities for the bubble cap (**8B**) and cone distributor (**8C**) are relatively invariant with axial position in that region (see Figure 22), the axial liquid velocities for the perforated-plate distributor (**8A**) exhibit a more significant variation with axial position. As observed here for the perforated-plate distributor, the distributor effect at high gas velocity of 12 cm/s at heights above two column diameters is unexpected and contrary to our other observations and those reported by researchers at Sandia National Laboratory (Shollenberger et al., 2000). At present, we cannot explain this anomaly. There is a possibility that, since the experiments discussed earlier were not performed in sequence, the physical/chemical properties of the air–water system for the perforated-plate distributor were different, due to the presence of impurity, and this caused different coalescence/redispersion behavior.

Comparison of CARPT with HPA and HFA Techniques

The objective of this section is to compare the results from CARPT measurements with independent experimental data. The data for the time-averaged liquid velocities and the turbulent (shear and normal) stresses have been compared. For the mean velocities, HPA experiments were conducted as part of this work to measure the time-averaged liquid velocities in a 19-cm-diameter column under operating conditions similar to that used for the CARPT experiments.

The HPA is a time-of-flow measurement technique used to determine the mean liquid velocity between two points in the flow field. It essentially measures the distribution of the passage time of fluid elements that start at one point in the flow and happen to pass by at another point downstream. This technique, in a sense, measures the residence-time density function of fluid elements between the emitter and sensor. By fitting the response measured by the sensor using a suitable model, the mean time of passage (or mean residence time) of the fluid elements can be deduced, from which the average velocity of the fluid between the sensor and the emitter is calculated. This technique therefore only provides an indirect measurement of the time-averaged liquid velocity between two points, and is based on the assumption that in a time-averaged sense, the emitter and sensor probes are positioned along the streamline of liquid motion. The details of the technique can be found in a study by Lubbert and Larson (1990) who used HPA to measure liquid velocities in fermenters.

The HPA experiments were conducted in the 19-cm-diameter column using distributor **8A**, for three gas velocities, 2 cm/s, 5 cm/s, and 12 cm/s, and static heights corresponding to those for the CARPT experiments given in Table 1.

A comparison of the 1-D axial liquid velocities from CARPT with those obtained from the HPA measurements is shown in Figure 23. At low gas velocity, that is, $U_g = 2$ cm/s, the data from two measurements agree very well. As the gas velocity increases, the liquid velocities from HPA are consistently lower than those measured by CARPT toward the center of the column, that is, $r \leq 4$ cm. In the outer annular region of the column, that is, $r \geq 4$ cm, the comparison between the two techniques is better, with slightly higher magnitudes of the liquid velocity shown by the HPA measurements, especially at the highest gas velocity. In general, it

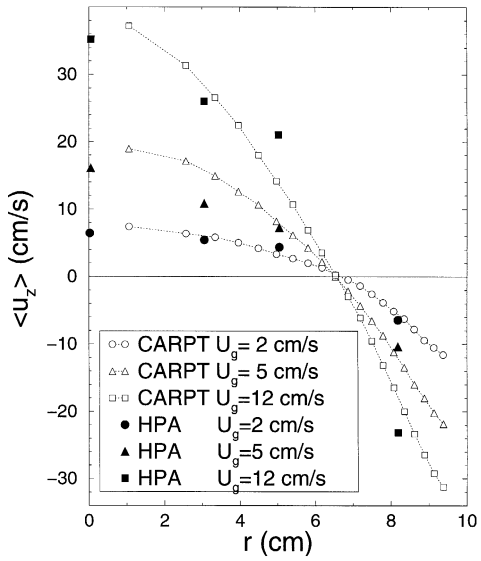

Figure 23. Comparison of CARPT and HPA measurements for the time-averaged axial liquid velocity; 19-cm column.

Distributor: 8A. The axial averaging range: $0.15H_D \leq z \leq 0.85H_D$. H_D is column's dynamic height.

seems that the results from HPA show flatter profiles for the axial liquid velocity than that of CARPT. Considering the nature of the HPA measurements, in terms of deducing the velocity from the time-of-flow data, rather than obtaining direct velocity measurements, the present agreement between the two techniques is considered satisfactory. The ability of CARPT to measure mean velocity has been confirmed by comparison with PIV (Chen et al., 1999).

Reynolds stress measurements from CARPT are compared with experimental data of Menzel et al. (1990), who used the HFA technique in the air–water system. The 14-cm-diameter column was chosen with distributor **6B**, which is similar to that used by Menzel et al. (1990). The superficial gas velocities were also chosen to match that of Menzel et al. (1990). Comparison of $\langle u_r' u_z' \rangle$ is shown in Figure 24. For two measurement techniques that are based on different principles of operation, the magnitudes of the correlation between the fluctuating velocities are rather close to each other. This provides a valuable substantiation of the CARPT technique for measurement of turbulence parameters. The largest discrepancy between the two sets of data is observed close to the wall of the column, where results from HFA are higher than those from CARPT. A possible reason for this difference could be that closer to the wall the CARPT particle tracer is not able to capture the higher frequencies of the liquid movement, which may contribute significantly to the flow in this region. On the other hand, it is also known that intrusive probes such as the HFA result in higher measurement errors close to the wall because of wall effects that interfere with the signal. Therefore, the discrepancy near the wall could be due to errors in both CARPT measurements and HFA. It is noteworthy that the comparison of the results from the two techniques is fairly good at lower gas velocity where HFA is known to be reliable. It is also known that HFA results at high gas holdup at high gas velocities can be subject to error.

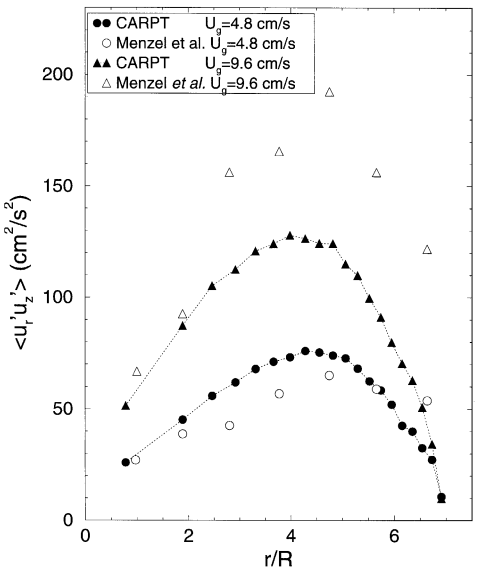

Figure 24. Comparison of Reynolds shear stress, $\langle u_r' u_z' \rangle$, based on CARPT and HFA data of Menzel et al. (1990).

The axial averaging range: $0.15H_D \le z \le 0.85H_D$. H_D is column's dynamic height.

The overall results suggest a modest to good comparison between the two techniques and hence provide an evaluation of the capability of CARPT to measure the turbulent shear stresses.

Conclusions

The quantitative analysis based on the Lagrangian velocity data obtained using the CARPT technique provides insight into the fluid dynamics of the liquid phase in 3-D cylindrical bubble columns operated with different gas distributors and at different superficial gas velocities. Important findings and conclusions are:

1. Disregarding the end zones, there is a statistically stationary liquid flow pattern in the bubble columns, where a mean liquid recirculation velocity profile can be seen. Such flow patterns are single-cell and axisymmetric about the column's axis. In this region, the time-averaged radial and azimuthal velocities are negligible in comparison with the axial velocity. This finding confirms the assertions made by Hill (1974), Yao et al. (1991), and others who used different experimental techniques.

2. The time-averaged liquid axial velocity and Reynolds stress profiles undergo a large change as the superficial gas velocity increases from 2.4 cm/s to 12 cm/s, which may indicate a flow regime change from bubbly to churn turbulent.

3. For all column sizes and superficial gas velocities, the inversion point of the mean liquid axial velocity profile is always located at $r/R \approx 0.65$. It roughly corresponds to the location of the maximum absolute value of the Reynolds shear stress, $-\rho_l \langle u_r' u_z' \rangle$.

4. The turbulence intensities are dominated by the normal stress in the axial direction.

5. Effects of gas distributors on the mean liquid velocity, Reynolds shear stress, and global gas holdup are observed at some operating conditions.

Acknowledgments

The authors would like to thank the Department of Energy for financial support under Grant DE FC2295PC95051. Our gratitude also goes to Exxon Research and Engineering Company (ERE) for providing the CARPT hardware and to Air Products & Chemicals (APCI) for providing the motivation for this work. One of the authors (S.D.) would like to especially thank Dr. B. A. Toseland from APCI and Dr. M. Chang from ERE for valuable discussions and comments.

Notation

D = column diameter, cm
g = gravitational constant, cm/s^2
p = pressure, g/(s^2·cm)
P = mean pressure, g/(s^2·cm)
R = column radius, cm
$\boldsymbol{u}$ = liquid-phase velocity vector, cm/s
U_g = superficial gas velocity, cm/s

Greek letters

ϵ = time-averaged local gas holdup
$\langle \epsilon \rangle$ = global gas holdup
ρ_l = liquid-phase material mass density, g/cm^3
ρ_g = gas-phase material mass density, g/cm^3
μ_l = liquid−phase dynamic viscosity, g/(cm·s)
σ = liquid−gas surface tension, g/s^2

Literature Cited

Cassanello, M., F. Larachi, A. Kemoun, M. H. Al-Dahhan, and M. P. Dudukovic, "Inferring Liquid Chaotic Dynamics in Bubble Columns using CARPT," 5th *Gas-Liquid-Solid Reactors Symp.*, World Congress of Chemical Engineering, Melbourne, Australia (2001).

Chaouki, J., F. Larachi, and M. P. Dudukovic, "Noninvasive Tomographic and Velocimetric Monitoring of Multiphase Flows," *Ind. Eng. Chem. Res.*, **36**, 4476 (1997).

Chen, J., A. Kemoun, M. H. Al-Dahhan, M. P. Dudukovic, D. J. Lee, and L.-S. Fan, "Comparative Hydrodynamics Study in Bubble Column Using Computer-Automated Radioactive Particle Tracking (CARPT)/Computed Tomography (CT) and Particle Image Velocimetry (PIV)," *Chem. Eng. Sci.*, **54**, 2199 (1999).

Chen, R. C., J. Reese, and L.-S. Fan, "Flow Structure in a Three-Dimensional Bubble Column and a Three-Phase Fluidized Bed," *AIChE J.*, **40**, 1093 (1994).

Deckwer, W. D., and A. Schumpe, "Improved Tools for Bubble Column Reactor Design and Scale-up," *Chem. Eng. Sci.*, **48**, 889 (1993).

Degaleesan, S., *Fluid-Dynamic Measurements and Modeling of Liquid Mixing in Bubble Columns*, DSc Thesis, Washington Univ., St. Louis, MO (1997).

Delhaye, J. M., "Hot Film Anemometry in Two Phase Flows," *Two Phase Flow Instrumentation*, *National ASME/AIChE Heat Transfer Conf.*, Minneapolis, p. 58 (1969).

Delnoij, E., F. A. Lammers, J. A. M. Kuipers, and W. P. M. van Swaaij, "Dynamic Simulation of Dispersed Gas-Liquid Two-Phase Flow Using a Discrete Bubble Model," *Chem. Eng. Sci.*, **52**, 1429 (1997).

Devanathan, N., D. Moslemian, and M. P. Dudukovic, "Flow Mapping in Bubble Columns Using CARPT," *Chem. Eng. Sci.*, **45**, 2285 (1990).

Devanathan, N., *Investigation of Liquid Hydrodynamics in Bubble Columns via Computer Automated Radioactive Particle Tracking (CARPT)*, DSc Thesis, Washington Univ., St. Louis, MO (1991).

Drew, D. A., "Mathematical Modeling of Two-Phase Flow," *Annu. Rev. Fluid Mech.*, **15**, 261 (1983).

Dudukovic, M. P., N. Devanathan, and R. Holub, "Multiphase Reactor: Models and Experimental Verification," *Rev. Inst. Francais du Petrole*, **46**, 493 (1991).

Dudukovic, M. P., F. Larachi, and P. L. Mills, "Multiphase Reactors —Revisited," *Chem. Eng. Sci.*, **54**, 1975 (1999).
Fan, L.-S., *Gas-Liquid-Solid Fluidization Engineering*, Series in Chemical Engineering, Butterworths, Boston (1989).
Franz, K., T. Borner, H. J. Kantorek, and R. Buchholz, "Flow Structures in Bubble Columns," *Ger. Chem. Eng.*, **7**, 365 (1984).
Geary, N., and R. G. Rice, "Circulation and Scale-Up in Bubble Columns," *AIChE J.*, **33**, 575 (1992).
Grienberger, J., and H. Hofmann, "Investigations and Modeling of Bubble Columns," *Chem. Eng. Sci.*, **47**, 2215 (1992).
Groen, J. S., R. F. Mudde, and H. E. A. van den Akker, "Time Dependent Behavior of the Flow in a Bubble Column," *Trans. Inst. Chem. Eng. Res. Des.*, **73** (A6), 615 (1995).
Groen, J. S., R. G. C. Oldeman, R. F. Mudde, and H. E. A. van den Akker, "Coherent Structures and Axial Dispersion in Bubble Column Reactors," *Chem. Eng. Sci.*, **51**, 2511 (1996).
Hammer, H., H. Schrag, K. Hektor, K. Schonau, W. Kuster, A. Soemarno, U. Sahabi, and W. Napp, "New Sub-Functions on Hydrodynamics, Heat and Mass Transfer for Gas/Liquid and Gas/Liquid/Solid Chemical and Biochemical Reactors," *Frontiers in Chemical Reaction Engineering*, L. K. Doraiswamy and R. A. Mashelkar, eds., Wiley, New York, p. 464 (1984).
Herringe, R. A., and M. R. Davis, "Detection of Instantaneous Phase Changes in Gas-Liquid Mixtures," *J. Phys. E: Sci. Instrum.*, **7**, 807 (1974).
Hills, J. H., "Radial Non-Uniformity of Velocity and Voidage in a Bubble Column," *Trans. Inst. Chem. Eng.*, **52**, 1 (1974).
Joshi, J. B., V. V. Ranade, S. D. Gharat, and S. S. Lele, "Sparged Loop Reactors," *Can. J. Chem. Eng.*, **68**, 705 (1990).
Kim, J., M. Parviz, and R. Moser, "Turbulence Statistics in Fully Developed Channel Flow at Low Reynolds Number," *J. Fluid Mech.*, **177**, 133 (1987).
Kreplin, H., and H. Eckelmann, "Behavior of the Three Fluctuating Velocity Components in the Wall Region of a Turbulent Channel Flow," *Phys. Fluids*, **22**, 1233 (1979).
Krishna, R., J. W. A. de Swart, J. Ellenberger, G. B. Martina, and C. Maretto, "Gas Holdup in Slurry Bubble Columns: Effect of Column Diameter and Slurry Concentrations," *AIChE J.*, **33**, 311 (1997).
Krishna, R., J. M. Van Baten, and M. I. Urseanu, "Three Phase Eulerian Simulations of Bubble Column Reactors Operating in the Churn Turbulent Regime: A Scale-Up Strategy," *Chem. Eng. Sci.*, **55**, 3275 (2000).
Kumar, S. B., *Computed Tomography Measurements of Void Fraction and Modeling of the Flow in Bubble Columns*, PhD Thesis, Florida Atlantic Univ., Boca Raton, FL (1994).
Kumar, S. B., N. Devanathan, D. Moslemian, and M. P. Dudukovic, "Effect of Scale on Liquid Recirculation in Bubble Columns," *Chem. Eng. Sci.*, **49**, 5637 (1994).
Kumar, S. B., W. B. Vanderheyden, N. Devanathan, T. Padial, M. P. Dudukovic, and B. A. Kashiwa, "Numerical Simulation and Experimental Verification of Gas-Liquid Flow in Bubble Columns," *Industrial Mixing Fundamentals with Applications, AIChE Symp. Ser. 305*, Am. Inst. Chem. Eng., New York, p. 11 (1995a).
Kumar, S. B., D. Moslemian, and M. P. Dudukovic, "A γ-Ray Tomographic Scanner for Image Voidage Distribution in Two-Phase Flow System," *Flow Meas. Instrum.*, **6**(1), 61 (1995b).
Kumar, S. B., M. P. Dudukovic, and B. A. Toseland, "Measurement Techniques for Local and Global Fluid Dynamic Quantities in Two and Three Phase Systems," *Non-Invasive Monitoring of Multiphase Flows*, Chap. 1, J. Chaouki, F. Larachi, and M. P. Dudukovic, eds., Elsevier, Amsterdam, p. 1 (1997a).
Kumar, S. B., D. Moslemian, and M. P. Dudukovic, "Gas Holdup Measurements in Bubble Columns Using Computed Tomography," *AIChE J.*, **43**, 1414 (1997b).
Lapin, A., and A. Lubbert, "Numerical Simulation of the Dynamics of Two-Phase Gas-Liquid Flows in Bubble Columns," *Chem. Eng. Sci.*, **49**, 3661 (1994).
Larachi, F., G. Kennedy, and J. Chaouki, "A γ-Ray Detection System for 3-D Particle Tracking in Multiphase Reactors," *Nucl. Instrum. Methods*, **A338**, 568 (1994).
Larachi, F., J. Chaouki, G. Kennedy, and M. P. Dudukovic, "Radioactive Particle Tracking in Multiphaase Reactors: Principles and Applications," *Non-Invasive Monitoring of Multiphase Flows*, Chap. 11, J. Chaouki, F. Larachi, and M. P. Dudukovic, eds., Elsevier, Amsterdam, p. 335 (1997).
Lin, J. S., M. M. Chen, and B. T. Chao, "A Novel Radioactive Particle Tracking Facility for Measurement of Solids Motion in Gas Fluidized Beds," *AIChE J.*, **31**, 465 (1985).
Lin, T.-J., J. Reese, T. Hong, and L.-S. Fan, "Quantitative Analysis and Computation of Two-Dimensional Bubble Columns," *AIChE J.*, **42**, 301 (1996).
Lubbert, A., and B. Larson, "Detailed Investigation of the Multiphase Flow in Airlift Tower Loop Reactors," *Chem. Eng. Sci.*, **45**, 3047 (1990).
Luo, H., and H. F. Svendsen, "Turbulent Circulation in Bubble Columns from Eddy Viscosity Distributions of Single Phase Pipe Flow," *Can. J. Chem. Eng.*, **69**, 1389 (1991).
Menzel, T., T. in der Weide, O. Staudacher, O. Wein, and U. Onken, "Reynolds Shear Stress for Modeling of Bubble Column Reactors," *Ind. Eng. Chem. Res.*, **29**, 988 (1990).
Moslemian, D., N. Devanathan, and M. P. Dudukovic, "Radioactive Particle Tracking Technique for Investigation of Phase Re-Circulation and Turbulence in Multiphase Systems," *Rev. Sci. Instrum.*, **63**, 4361 (1992).
Mudde, R. F., D. J. Lee, J. Reese, and L.-S. Fan, "Role of Coherent Structures on Reynolds Stresses in a 2-D Bubble Column," *AIChE J.*, **43**, 913 (1997a).
Mudde, R. F., J. S. Groen, and H. E. A. Van Den Akker, "Role of Coherent Structures on Reynolds Stresses in a 2-D Bubble Column," *Chem. Eng. Sci.*, **52**, 4217 (1997b).
Nottenkamper, R., A. Steiff, and P.-M. Weinspach, "Experimental Investigation of Hydrodynamics of Bubble Columns," *Ger. Chem. Eng.*, **6**, 147 (1983).
Pan, Y., M. P. Dudukovic, and M. Chang, "Dynamic Simulation of Bubbly Flow in Bubble Columns," *Chem. Eng. Sci.*, **54**, 2481 (1999).
Pan, Y., M. P. Dudukovic, and M. Chang, "Numerical Investigation of Gas-Driven Flow in Two-Dimensional Bubble Columns," *AIChE J.*, **46**, 434 (2000).
Ranade, V. V., "Flow in Bubble Columns: Some Numerical Experiments," *Chem. Eng. Sci.*, **47**, 1857 (1992).
Reilly, I. G., D. S. Scott, T. J. W. de Bruin, A. Jain, and J. Piskorz, "Correlation for Gas Holdup in Turbulent Coalescing Bubble Columns," *Can. J. Chem. Eng.*, **64**, 705 (1986).
Sanyal, J., S. Vasquez, S. Roy, and M. P. Dudukovic, "Numerical Simulation of Gas-Liquid Dynamics in Cylindrical Bubble Columns," *Chem. Eng. Sci.*, **54**, 5071 (1999).
Saxena, S. C., "Bubble Column Reactors and Fischer-Tropsch Synthesis," *Catal. Rev. -Sci. Eng.*, **37**(2), 227 (1995).
Serizawa, A., I. Kataoka, and I. Michiyoshi, "Turbulence Structure of Air-Water Bubbly Flow—I. Measuring Techniques," *Int. J. Multiphase Flow*, **2**, 221 (1975).
Shah, Y. T., B. G. Kelkar, S. P. Godbole, and W. D. Deckwer, "Design Parameter Estimations for Bubble Column Reactors," *AIChE J.*, **28**, 353 (1982).
Shollenberger, K. A., J. R. Torczynski, and D. L. George, "Effect of Sparger Geometry on Gas Volume-Fraction in Bubble Column Flows Measured by Gamma-Densitometry Tomography (GDT)," AIChE Meeting, Los Angeles, CA (2000).
Sokolichin, A., and G. Eigenberger, "Gas-Liquid Flow in Bubble Columns and Loop Reactors: Part 1. Detailed Modelling Numerical Simulation," *Chem. Eng. Sci.*, **24**, 5735 (1994).
Sokolichin, A., G. Eigenberger, A. Lapin, and A. Luebbert, "Dynamic Numerical Simulation of Gas-Liquid Two-Phase Flows, Euler/Euler versus Euler/Lagrange," *Chem. Eng. Sci.*, **52**, 611 (1997).
Svendsen, H. F., H. A. Jakobsen, and R. Torvik, "Local Flow Structures in Internal Loop and Bubble Column Reactors," *Chem. Eng. Sci.*, **45**, 2325 (1992).
Tennekes, H., and J. L. Lumley, *A First Course on Turbulence*, The MIT Press, Cambridge (1972).
Tzeng, Y. B., R. C. Chen, and L.-S. Fan, "Visualization of Flow Characteristics in a 2-D Bubble Column and Three-Phase Fluidized Bed," *AIChE J.*, **39**, 733 (1993).
Ueyama, K., and T. Miyauchi, "Properties of Recirculating Turbulent Two Phase Flow in Gas Bubble Columns," *AIChE J.*, **25**, 258 (1979).
Yang, Y. B., N. Devanathan, and M. P. Dudukovic, "Liquid Backmixing in Bubble Columns," *Chem. Eng. Sci.*, **47**, 2859 (1992).
Yao, B. P., C. Zheng, H. E. Gasche, and H. Hofmann, "Bubble Behavior and Flow Structure of Bubble Columns," *Chem. Eng. Process.*, **29**, 25 (1991).

Manuscript received Dec. 6, 1999, and revision received Mar. 20, 2001.